UC Davis

UC Davis Previously Published Works

Title

Strain localization instabilities and the genesis of multiple axes of seafloor spreading in the Carmen basin, southern Gulf of California

Permalink

https://escholarship.org/uc/item/5kb0h6jd

Journal

International Journal of Earth Sciences, 113(5)

ISSN

1437-3254

Authors

Julià-Miralles, Marc

Yarbuh, Ismael

Spelz, Ronald M

et al.

Publication Date

2024-07-01

DOI

10.1007/s00531-024-02426-6

Peer reviewed

eScholarship.org Powered by the California Digital Library
University of California

International Journal of Earth Sciences
https://doi.org/10.1007/s00531-024-02426-6

ORIGINAL PAPER

Strain localization instabilities and the genesis of multiple axes of seafloor spreading in the Carmen basin, southern Gulf of California

Marc Julià-Miralles[1] · Ismael Yarbuh[2] · Ronald M. Spelz[2] · Raquel Negrete-Aranda[3] · Juan Contreras[4] · John M. Fletcher[5] · Antonio González-Fernández[5] · Robert Zierenberg[6] · David W. Caress[7]

Received: 29 November 2023 / Accepted: 29 April 2024
© The Author(s) 2024

Abstract

We present new insight into the tectonic evolution of the Carmen basin (CB) in the southern Gulf of California (GC) from high-resolution bathymetry and two-dimensional seismic reflection data. Our goal is to document the seafloor morphology and sub-surface acoustic characteristics to understand the structure and crustal lithology across the CB. We identify three sub-basins with distinct geometries and evolutionary histories, with basement structures displaying a strong affinity with highly reflective, sigmoidal-shaped layers and the emplacement of high-amplitude tabular material underlying sediments with varying stratigraphic thicknesses. From the extent of new oceanic crust accreted along the CB, we estimate the age of the basin using a seafloor spreading rate of 52 mm/year, which is the average velocity of the relative plate motion between the Baja California microplate and the North American plate, as documented by previous authors. The southern and central sub-basins of the CB are mainly abandoned, while the northern one is currently the locus of seafloor spreading. This is evidenced by the juxtaposition of oceanic crust younger than ~ 1.9 Ma against older oceanic crust correlating in age with the adjacent Guaymas and Farallon basins to the northeast and southwest, respectively. We propose that mantle upwelling beneath the CB is a northward continuation of the East Pacific Rise, resulting in a fast-evolving system with sharp variations in strain localization within the seafloor spreading centers of the CB.

Keywords High-resolution bathymetry · Seismic reflection profiles · Basin structure · Crustal lithology · Fault kinematics

Introduction

Despite recent progress in understanding the rifting dynamics of the Gulf of California (GC), significant gaps in information still exist due to extensive unexplored regions (Lonsdale 1989; Aragón-Arreola et al. 2005; González-Fernández et al. 2005; Aragón-Arreola and Martín-Barajas 2007; Lizarralde et al. 2007; González-Escobar et al. 2010; Contreras-Pérez et al. 2012; Martín-Barajas et al. 2013; Ramírez-Zerpa et al. 2022). This lack of information hinders our ability to establish a comprehensive context for the kinematics responsible for the opening of the GC, especially in the case of the pull-apart basins in the southern GC (Fig. 1), where geological data are still missing or has

✉ Ismael Yarbuh
uyarbuh@uabc.edu.mx

[1] Posgrado en Oceanografía Costera, Facultad de Ciencias Marinas, Universidad Autónoma de Baja California, Ensenada, Baja California, México

[2] Departamento de Geología, Facultad de Ciencias Marinas, Universidad Autónoma de Baja California, Ensenada, Baja California, México

[3] Investigadora Por México CONAHCYT, Laboratorio de Tectonofísica y Flujo de Calor, Centro de Investigación Científica y de Educación Superior de Ensenada (CICESE), Ensenada, Baja California, México

[4] Laboratorio de Tectonofísica y Flujo de Calor, Centro de Investigación Científica y de Educación Superior de Ensenada (CICESE), Ensenada, Baja California, México

[5] Departamento de Geología, Centro de Investigación Científica y de Educación Superior de Ensenada, Ensenada, Baja California, México

[6] Earth and Planetary Sciences, University of California, Davis, CA, USA

[7] Monterey Bay Aquarium Research Institute, Moss Landing, CA, USA

Published online: 21 May 2024

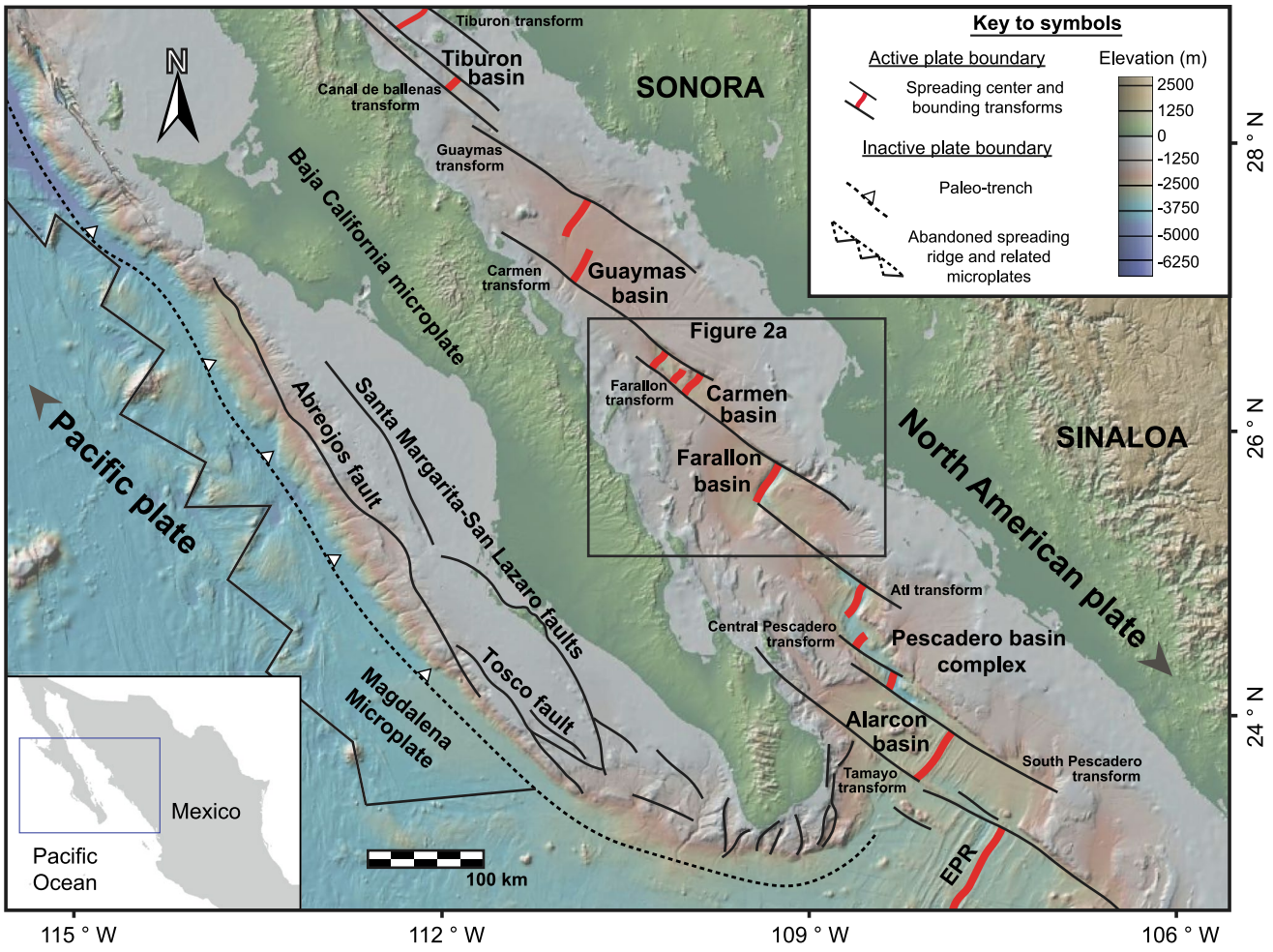

Fig. 1 Regional tectonic map of the southern Gulf of California showing plate motion (black arrows), transform fault system (black lines), pull-apart basins, and spreading centers (red lines). The Carmen basin is indicated by the black box (Fig. 2). The location of the paleo-trench and the partially subducted Magdalena microplate derived from the Farallon plate is marked by a black dashed line along the western margin of the Baja peninsula. The abbreviation EPR is used for the East Pacific Rise. Base map sourced from GeoMapApp (http://www.geomapapp.org)

poor spatial/temporal resolution (Sutherland et al. 2012 vs. Martín-Barajas et al. 2013).

It is known that the continental margins of the GC are highly extended and influenced by the development of low-angle master faults. These faults facilitate the isostatic rebound of the tectonically unloaded (ductile) lower plate and the formation of antiformal bulges that migrate in the direction of displacement of the (brittle) upper plate (Buck 1988; Wernicke and Axen 1988; Lavier et al. 1999; Fletcher and Spelz 2009). Local conditions that favor the development of such low-angle structures include a thinned lithosphere and a high extension rate, which result in higher-than-normal heat flow values (Buck 1988, 1993). Active rifting across the southwestern margin of the GC (Umhoefer et al. 2020) has also been associated with east-directed low-angle normal faults and simple shear deformation, accommodating significant crustal extension (Fletcher et al. 2000, 2003; Fletcher and Munguia 2000; Bot et al. 2016). In this region, strain results in ~ 40 km of linear extension toward the continental–oceanic crust transition, across the continental shelf of the Baja California peninsula (Fig. 1; Macias-Iñiguez et al. 2019).

According to Fornari et al. (1989), intra-transform spreading centers are a specific type of pull-apart basin found on oceanic transform faults, characterized by the development of short spreading centers surrounded by oceanic crust. Thus, oceanic transforms play a crucial role in the geology of mid-oceanic spreading ridges, where tectonic plates laterally move past each other, creating conditions conducive to the formation of intra-transform spreading centers (Gregg et al. 2006). These basins essentially consist of depressed regions between two offset segments of the mid-oceanic ridge, floored by oceanic crust (Mann et al. 2007). Therefore, oceanic transforms at mid-oceanic spreading ridges

give rise to pull-apart basins floored by oceanic crust, resembling those observed in the Siqueiros and Garret transform faults on the East Pacific Rise (Pockalny et al. 1997; Gregg et al. 2007).

In this research, we aim to establish a kinematic evolution model of the Carmen basin (CB; Figs. 1 and 2) using two-dimensional (2D) seismic reflection profiles and high-resolution bathymetry collected by Centro de Investigación Científica y de Educación Superior de Ensenada, Baja California (CICESE), Scripps Institution of Oceanography at the University of California San Diego (UCSD), and the Schmidt Ocean Institute (SOI) in 2006 and 2021, respectively. Here, we characterize the geometry and structure of the CB to identify: (i) different stages of crustal deformation, (ii) the basement lithology, (iii) the seismic stratigraphy, and (iv) the magmatic events preserved in the stratigraphy of the basin. Additionally, we compare our results against other neighboring basins in the southern GC using geological data (Duque-Trujillo et al. 2014, 2015; Umhoefer et al. 2020), seismic reflection images (Lizarralde et al. 2007; Piñero-Lajas 2008; Sutherland et al. 2012; Kluesner 2011; Kluesner et al. 2014; Macias-Iñiguez et al. 2019; Ramírez-Zerpa et al. 2022), mantle tomography data (Wang et al. 2009; Di Luccio et al. 2014; Ferrari et al. 2018), and analog modeling of pull-apart basins (van Wijk et al. 2017; Wu et al. 2009; Farangitakis et al. 2021) to reconstruct the structural evolution of this segment of the southern GC rift system. Finally, we discuss how the opening of the GC contributes to the formation of new oceanic crust, how the oceanic lithosphere is deformed to accommodate younger spreading centers, and the kinematics of the transform faults that currently make up the boundary between the Pacific and North American plates.

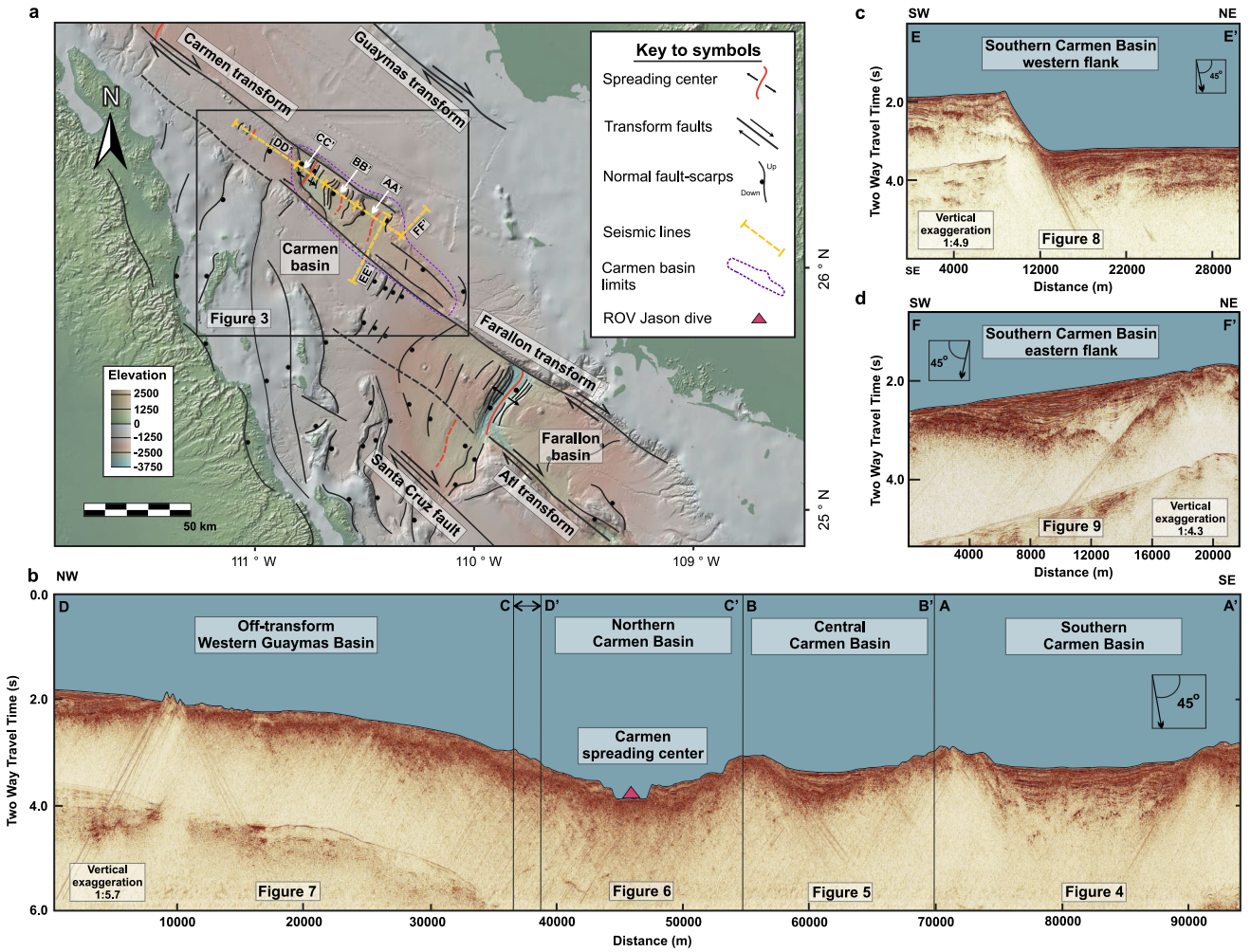

Fig. 2 **a** Regional tectonic map of the Carmen basin (CB), with labeled master transform faults (black). Multichannel seismic profiles are indicated by yellow lines. The black box corresponds to the CB shown in Fig. 3. Base map sourced from GeoMapApp (http://www.geomapapp.org). **b–d** 2D multichannel seismic reflection data across the CB. Seismic lines are divided by vertical black lines corresponding to Figs. 4–9

Tectonic evolution of the Gulf of California

The northwestern continental margin of Mexico is a good example of a transition from a convergent plate boundary to an oblique-divergent margin. During the Paleogene, the Farallon oceanic plate subducted beneath North America, and a divergent boundary between the Farallon plate and the approaching Pacific plate existed near the Baja California paleo-trench (Fletcher et al. 2007; Balestrieri et al. 2017). In the Eocene, the Farallon plate was consumed, and part of the East Pacific Rise (Atwater 1970) neared the paleo-trench. During the Oligocene, the East Pacific Rise directly interacted with the paleo-trench and the North American plate (Atwater 1989; Stock and Hodges 1989; Bunge and Grand 2000; Wright et al. 2016), leading to the breakup of the Farallon plate as the Pacific–Farallon spreading center approached North America (Wright et al. 2016).

The proximity of the Pacific–Farallon divergent margin to the continental borderland marked the end of Neogene subduction, initiating lithospheric extension and dextral shearing along the Magdalena plate boundary derived from the Farallon plate. Intraplate magmatism occurred along the Baja California peninsula due to viscous shearing (i.e., Tosco-Abreojos-Santa Margarita–San Lazaro fault zone; Fig. 1; Spencer and Normark 1979; Atwater and Stock 1998; Negrete-Aranda et al. 2013). In the early Miocene, the Farallon plate fragmented into several small plates, including the Guadalupe and Magdalena microplates, which, together with a section of the North American plate (i.e., California and Baja California peninsula), became coupled with the Pacific Plate (Wang et al. 2013) and started moving northwestward (Fig. 1; Nicholson et al. 1994; Bohannon and Parson 1995).

Dextral-oblique shearing migrated eastward from the continental margin into the current GC (Umhoefer et al. 2020). Crustal thinning in this region was permitted by a regional east-directed detachment system running along the Baja California peninsula and Sinaloa rifted margins (Ferrari et al. 2018). Eventually, brittle/ductile deformation (McKenzie 1978) became localized into the present-day GC. Simple-shear tectonics and crustal extension of the upper plate, decoupled from the lower crust, led to isostatic compensation, mantle upwelling, and the intrusion of dykes and sills, facilitating the breakup of the continental crust (Wernicke 1981). This process, accompanied by increased rift obliquity, facilitated plate boundary localization, marine incursion in the northern GC, and the formation of shallow water basins during the upper Miocene (Bennett et al. 2016; Umhoefer et al. 2018). The current tectonic regime, established in the early Pliocene, involved the East Pacific Rise extending into the GC (Wang et al. 2009, 2013), separating the Baja California peninsula from the North American continent as new oceanic crust surfaced in the southern GC (Lizarralde et al. 2007), permitted by right-lateral, right-stepping transform faults (Fletcher et al. 2007).

Methods

New high-resolution bathymetry data for the CB were collected during the FK210922 expedition in October 2021 aboard the R/V *Falkor*, operated by the Schmidt Ocean Institute (SOI). The data were acquired using an EM 302 multibeam echo sounder at a 30-kHz frequency, capturing up to 864 soundings with dual swath mode. This enabled detailed seabed mapping along the entire CB basin axis at 40-m intervals. The survey lines were spaced 5 km apart, running subparallel to the master transform faults that bound the basin. Data collection occurred at an average ship speed of 8 knots.

To study the rift evolution of the CB, we analyzed ~ 160 km of 2D seismic reflection data collected in 2006 aboard the R/V *Francisco de Ulloa* during a collaborative effort involving Centro de Investigación Científica y de Educación Superior de Ensenada, Baja California (CICESE), and Scripps Institution of Oceanography at the University of California, San Diego (UCSD). The seismic data, labeled AA'–FF' (Fig. 2) included a 108 km section (AA'–DD') parallel to the CB axis, along with two perpendicular sections, EE' (30 km long) and FF' (22 km long).

The seismic reflection data were processed using the open-source Seismic Unix software (https://wiki.seismicunix.org/start). We applied a three-stage workflow to generate sub-surface seismic reflection images: pre-stack, stack, and post-stack processing (Sheriff and Geldart 1995; Yilmaz 2001). This workflow enabled frequency extraction, multiple mitigation, signal amplitude equalization, noise reduction, precise ray trajectory correction, and spurious effect attenuation (Sheriff and Geldart 1995; Yilmaz 2001). Detailed documentation explaining the complete processing workflow is provided in the supplementary material that accompanies this paper.

Well-proven criteria, such as the continuity/variability of reflections, seismic character, and internal geometry of reflectors, were used to identify key structural features such as fault planes, folds, grabens, and sedimentary sequences. Quantitative parameters, including fault length and dip, striatal thicknesses, subsidence, and sedimentary sequence boundaries, were also determined (e.g., maximum flooding surfaces, erosion surfaces, and correlatable surfaces). Seismic facies analysis enabled the identification of basement lithology and sedimentary material, including magmatic injections and geothermal fluids, usually in the form of mosaic patterns of highly reflective surfaces (e.g.,

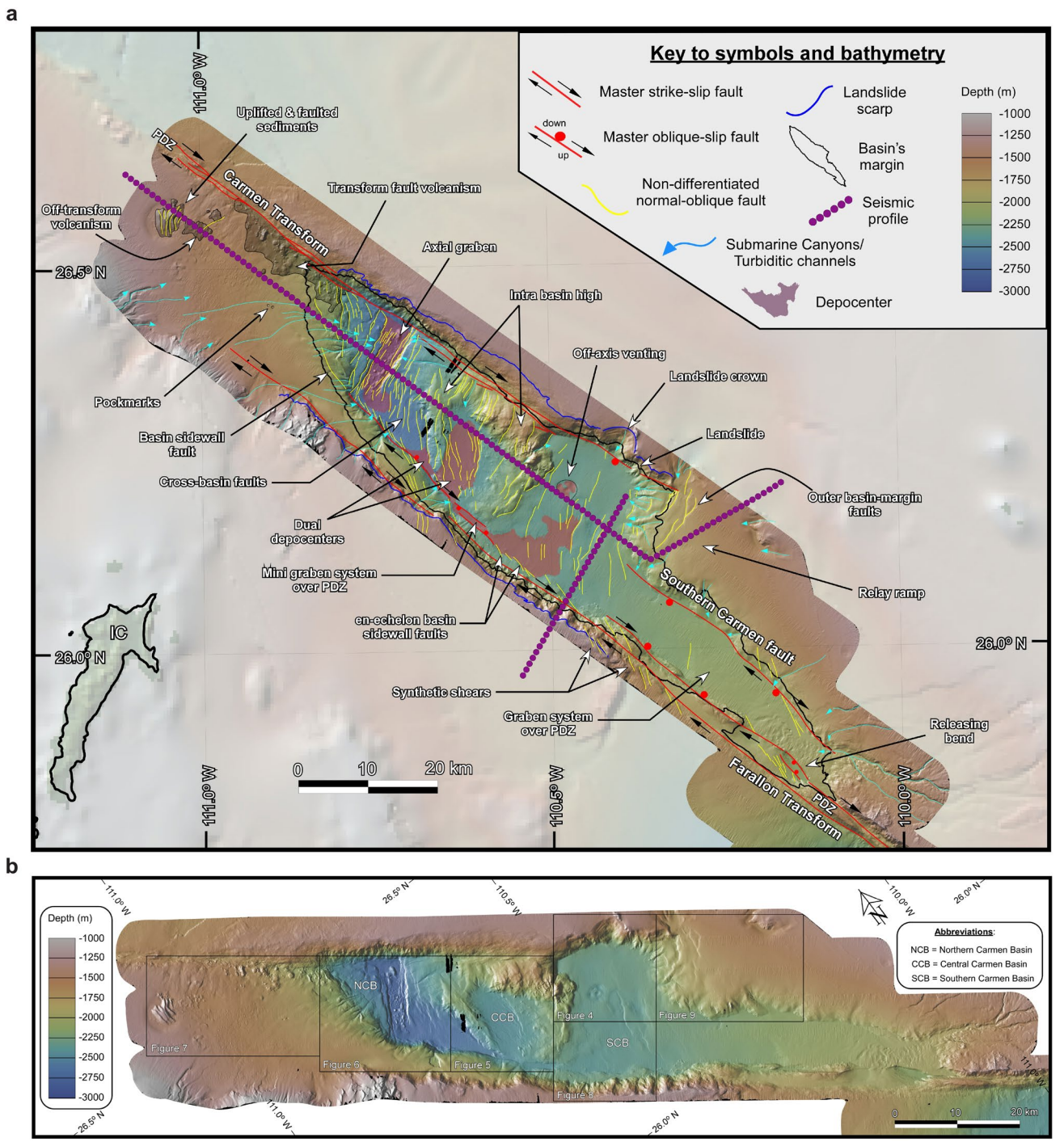

Fig. 3 **a** Structural map of the Carmen basin (CB) illustrating the two-dimensional architecture and geometry. High-resolution (40 m) bathymetry is overlaid on faded Global Multi-Resolution Topography (GMRT) bathymetry. The map reveals a series of depocenters within the CB, with increasing depth from south to north. These sub-basins are bounded by two master strike-slip transform faults (red lines), connected by an array of cross-basin faults (yellow lines). The current seafloor spreading center is located in the northern part of the CB. **b** Raw image displaying the high-resolution bathymetry of the CB, and the locations of other referenced figures

saucer-shaped sills; Polteau et al. 2008) and low-reflectance surfaces (e.g., dim spots; Chopra and Marfurt 2007).

Results

Geomorphology and 2D architecture of the Carmen basin

The newly collected bathymetric data (Fig. 3) reveal that the CB is a narrow, rhomboidal pull-apart basin developed between two dextral transform faults. The basin measures 100 km in length and 20 km in width, yielding a length-to-width ratio of 5:1 (Fig. 3). Two sub-parallel, northwest-oriented principal displacement zones control the northeastern and southwestern margins of the CB. The Carmen transform fault extends 150 km, while the Farallon transform in the southwest stretches 200 km. These bounding zones overlap and connect through a transverse system of en-echelon oblique-extensional normal faults, creating three distinct sub-basins. The northernmost graben hosts the current seafloor spreading center measuring ~ 12 km in length (Fig. 3).

The bathymetry of the CB reveals significant footwall uplift of the outer margin along the trace of the transform faults. This nearly vertical uplift is accommodated by an array of en echelon segmented basin sidewall faults developed on both flanks of the CB (Fig. 3). Along these steep faults, gravitational instabilities develop, leading to rapid and episodic slumping and grain flows, forming distinct cliffs with landslide crowns and scarps along the basin's outer margin (Fig. 3). Yet, the primary sediment routing system for infilling the CB appears to be a submarine dendritic drainage system originating from the tips of the principal displacement zones (Fig. 3).

At a finer scale, Fig. 3 reveals a cross-basin fault system that propagates obliquely to the principal displacement zones. This fault system induces a left-stepping arrangement of synthetic Riedel shear faults (Christie-Blick and Biddle 1985; Wu et al. 2009) that curve into an elongated sigmoidal shape, connecting the sidewall faults at both sides of the basin. The resulting horst–graben structure divides the CB into three distinct sub-basins with contrasting morphologies (Fig. 3): (i) the southern CB, (ii) the central CB, and (iii) the northern CB. Further details on these sub-basins are provided in the following paragraphs.

Southern CB: The sub-basin features the shallowest depocenter (~ 2200 mbsl) among all the sub-basins. It has a length of ~ 20 km and a width of ~ 23 km. The basin is delimited by an array of cross-basin faults, oriented at a high angle to the bounding transform faults (Fig. 3). The northern margin is bounded by an uplifted and translated crustal block, while the southern margin is delimited by a strike-slip relay ramp that transfers and accommodates the deformation between the Carmen transform fault and a secondary oblique-slip fault, which we refer to as 'Southern Carmen fault' (Fig. 3). The NW-striking Carmen transform fault terminates abruptly against an array of NE–SW striking normal faults developed over the relay ramp on the outer basin-margin of the sub-basin (Fig. 3). The relay ramp lies on the footwall of the oblique Southern Carmen fault, which controls a prominent graben system with a length of ~ 40 km and a width of ~ 15 km in the southeastern corner of the CB.

The graben system is parallel to the Pacific–North American plate boundary (Fig. 1) and occurs along the divergent-wrench principal displacement fault zone associated with the Farallon transform. The graben is heavily sedimented and poorly cut by secondary faults traversing the smooth valley floor. The limited number of cross-basin fault scarps indicates their potential erosion or burial under the relatively thick layer of sediments derived from a dense network of drainages and submarine canyons that convey sediments to the southeastern portion of the basin (Fig. 3). However, a small pull-apart basin, resulting from a releasing bend along the Farallon's right-lateral principal displacement zone, indicates ongoing tectonic stresses and the formation of an embryonic graben system in the southern corner of the basin (Fig. 3). In the central portion of the southern CB, a circular feature with a diameter of ~ 3 km is interpreted as an area of off-axis venting a small depression formed as a result of the seepage of fluids and gasses through the seafloor and into the hydrosphere (Teske et al. 2020).

Central CB: The sub-basin is located at a depth of ~ 2400 mbsl. It has a length of ~ 20 km and a width of ~ 18 km. This structure acts as a connection between the northern and the southern CB. It is bordered by two intra-basin highs that have formed in response to a series of cross-basin faults that originate from synthetic Riedel shears (Wu et al. 2009) along the basin's sidewalls, connecting the master transform faults on each side of the CB (Fig. 3). These structural highs can be attributed to block translation and rotation during the early stages of basin development. The geometry of the central CB is elongated and oval, with a northern orientation, suggesting that deformation may have ceased in this region, allowing its spreading center to migrate northwestward toward the northern CB (Fig. 3). Variations in the topography of the central CB indicate the juxtaposition of different materials, with structural highs representing either a crystalline basement or possibly volcanic activity (Fig. 3). Conversely, the subsided depocenter likely consists of sedimentary material derived from local and distant sources, including gravitational mass movements and submarine contour currents (Fig. 3).

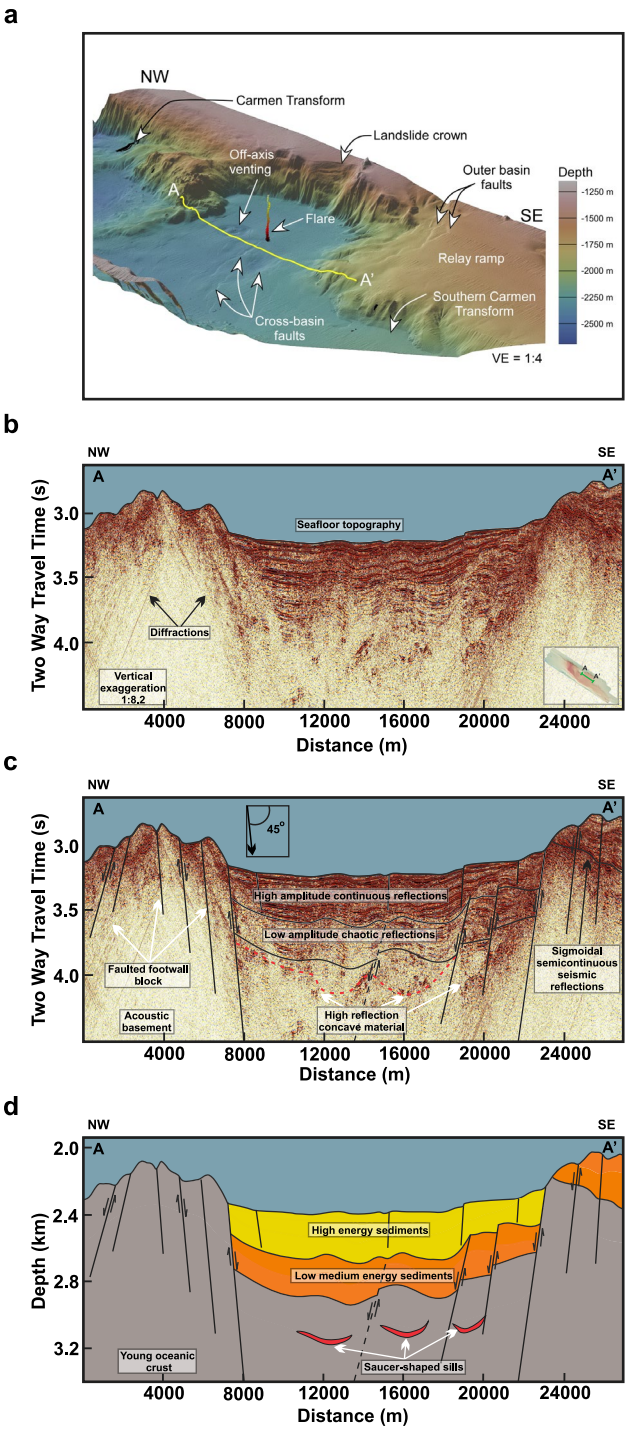

Fig. 4 Seismic profile A–A' across the southern Carmen basin (SCB). **a** Perspective 3D view of the 40-m resolution bathymetry of the SCB, generated in Canvas Xgeo (https://www.canvasgfx.com). VE = vertical exaggeration. The flare (acoustically imaged gas bubble plum) emerging from the seafloor was imaged using the Interactive Visualization Systems (IVS) Fledermaus 8.4.2 software package (www.qps.nl). **b** Raw seismic image. **c** Structural and stratigraphic seismic interpretation. **d** Interpreted geologic cross section. Depth in panel **d** was converted from Two Way Travel Time to meters assuming a seismic velocity of 1500 m s^{-1} (see also the supplementary material that accompanies this paper). The seismic image reveals a wide, symmetrical graben bounded by two primary normal faults, identified as cross-basin structures (Fig. 3). The subsidence created by these faults leads to 0.73 s of TWTT (~550 m) of sedimentary sequences deposited above an acoustic basement interpreted as a young oceanic crust. Panel **c** highlights high-amplitude reflections at a depth of 4.15 s, possibly indicating an ancient spreading center near abandoned nested normal faults. The dashed red line shows the location of magmatic intrusion interpreted as saucer-shaped sills. Low-amplitude facies in the seismic data may indicate fluid or gas migration toward the seafloor, as shown in the flare in panel **a**

Northern CB: The sub-basin is located in the deepest part of the entire CB, reaching depths of ~ 2800 mbsl. It has a length of ~ 20 km and a width of ~ 20 km. The basin exhibits a broad nested graben where rocks have undergone downward displacement along an array of cross-basin faults connecting the bounding master faults (Fig. 3). The overall geometry and geomorphological features of the northern CB suggest that the basin has evolved due to transtensional deformation (Wu et al. 2009), similar to the Pescadero basin complex located further southeast (Ramírez-Zerpa et al. 2022). The northern CB hosts the current seafloor spreading center, featuring a short and narrow axial graben oriented sub-perpendicular to the principal displacement zones. In 2008, the Woods Hole Oceanographic Institution's ROCA expedition aboard the R/V *Atlantis* utilized the remotely operated vehicle (ROV) *Jason* to conduct a dive into the CB axial graben (Fig. 2). During this dive, pillow basalts (ROCA 9J-10) were sampled within the active axis of CB as reported by Kluesner et al. (2011). Unlike the uplifted ramps that bound the opposite sides of the basin, the median valley floor is poorly sedimented and displays an irregular topography with rounded volcanic mounds (Fig. 3). Magmatic activity is conspicuous not only across the spreading center but also along the bounding master faults, as well as in the elevated areas within the sub-basins. Extensive volcanic bodies can also be observed at the northern termination of the Carmen transform fault (Fig. 3). Within this area, we identify a distinct feature that emerges on the seafloor, characterized by uplifted and faulted sediments, which in turn are often associated with off-axis magmatism (Teske et al. 2020).

Seismic interpretation of the Carmen basin

The seismic interpretation of lines AA'–FF' (Figs. 4, 5, 6, 7, 8, 9) and morphological analysis in Fig. 3 reveal the structural evolution of the CB. At a larger scale, the sub-basins exhibit three distinct seismic facies (Figs. 4, 5, 6, 7, 8, 9). From base to top in the seismic sections, the first seismic facies is interpreted as the acoustic basement, characterized

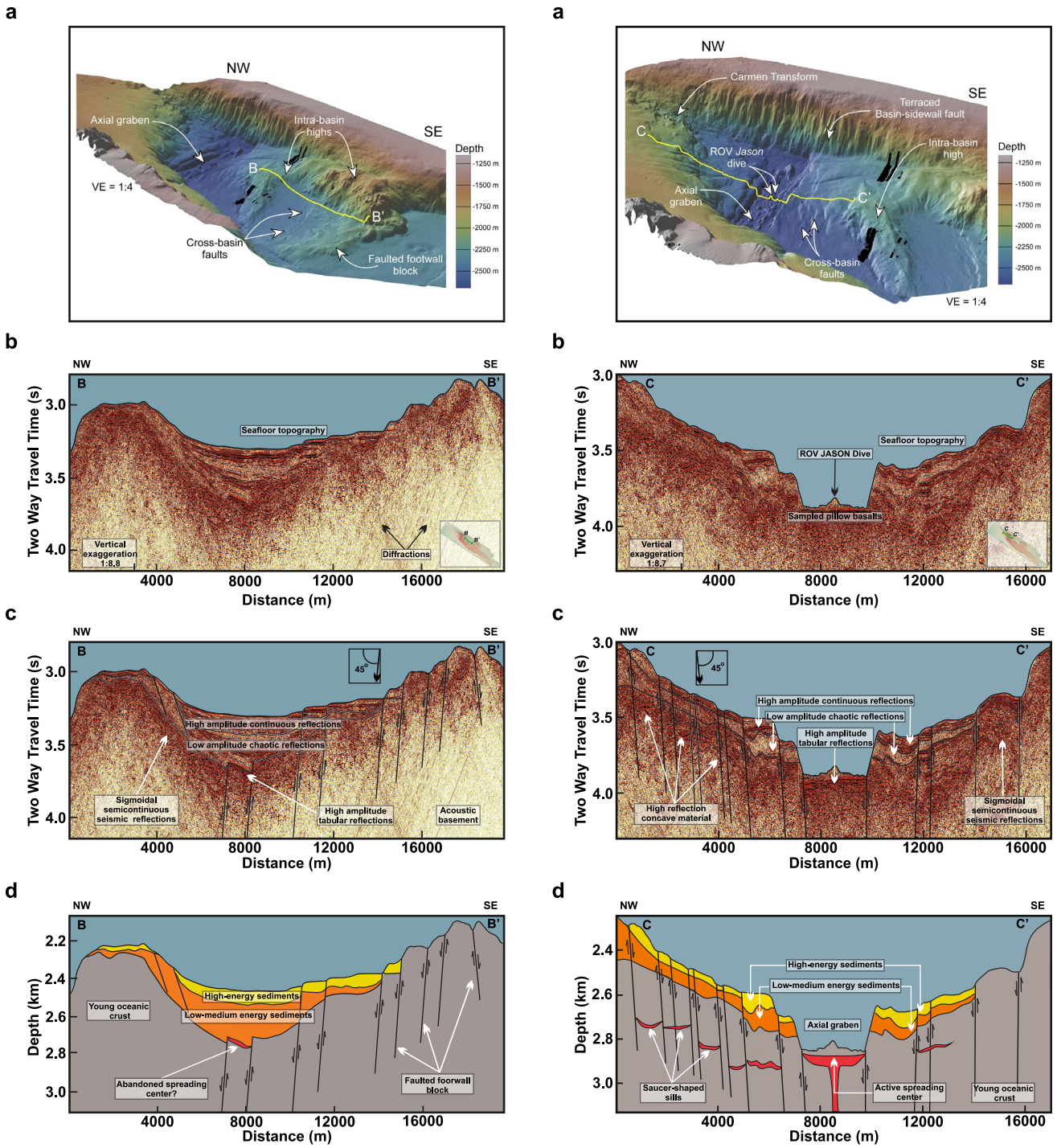

Fig. 5 Seismic profile B–B' across the central Carmen basin (CCB). **a** Perspective 3D view of the 40-m resolution bathymetry of the CCB, generated in Canvas Xgeo (https://www.canvasgfx.com). **b** Raw seismic image. **c** Structural and stratigraphic seismic interpretation. **d** Interpreted geologic cross section. The image reveals an asymmetrical half-graben structure NW-striking normal faults accommodating 0.40 s (~300 m) of syn-tectonic sedimentation. In panel **c**, at a depth of 3.73 s, tabular high-amplitude reflections suggest the presence of an ancient spreading center, similar to Fig. 4

Fig. 6 Seismic profile C–C' across the northern Carmen basin (NCB). **a** Perspective 3D view of the 40-m resolution bathymetry of the NCB, generated in Canvas Xgeo (https://www.canvasgfx.com). ROV = remotely operated vehicle; VE = vertical exaggeration. **b** Raw seismic image. **c** Structural and stratigraphic seismic interpretation. **d** Interpreted geologic cross section. The profile intersects the axial graben of the northern CB. The spreading center is interpreted as an asthenospheric mantle reaching the seafloor to generate new ocean crust

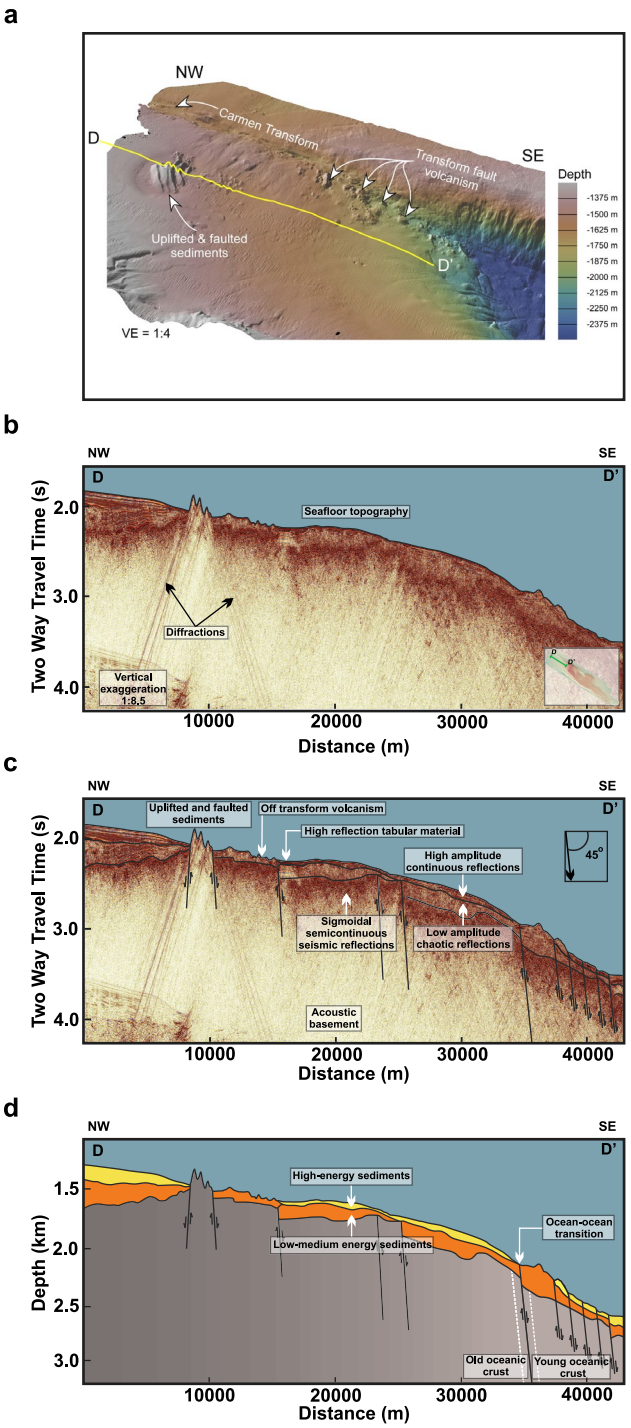

Fig. 7 Seismic profile D–D' spans the northernmost part of the Carmen basin (CB) **a** Perspective 3D view of the 40-m resolution bathymetry, generated in Canvas Xgeo (https://www.canvasgfx.com). **b** Raw seismic image. **c** Structural and stratigraphic seismic interpretation. **d** Interpreted geologic cross section. The seismic data reveal buried faults beneath sediments, indicating their potential older age compared to the normal faults in the CB. The basement extends along the entire seismic profile at depths between 2.27 and 3.1 s of TWTT (~1700 and 2100 mbsl). It is interpreted that this material is of volcanic origin, evident from seismic reflections exhibiting good lateral continuity and ropey-like high-amplitude features. Notably, a significant seismic feature is a submarine hill toward the NW (Fig. 3), suggesting it is the youngest feature of the section

by reflective, ropey-like layers with sigmoidal, semi-continuous reflections and strong lateral coherence. Below this layer, the acoustic basement continues at depth as reflections under which seismic signals are no longer received, thus in the seismic sections, these areas are attenuated (Figs. 4, 5, 6, 7, 8, 9). These rocks are interpreted as volcanic flows spanning a depth range from 3.87 to 2.27 s (s) of Two Way Travel Time (TWTT). Assuming a seismic velocity of the sea bottom reflection of 1500 m s^{-1}, we estimate that the depth of the acoustic basement varies between 2900 and 1700 m (Figs. 4, 5, 6, 7, 8, 9). The two seismic facies overlying the acoustic basement represent sedimentary layers filling the basin. The underlying facies consists of sequences with alternating medium and low-energy chaotic reflections, resembling accumulations of inter-glacial diatomaceous muds (Kluesner 2011; Kluesner et al. 2014). The overlying facies consists of sequences with alternating medium and high-energy coherence reflections, displaying diatomaceous mud and sand turbidites deposited in a high-energy environment (Kluesner 2011; Kluesner et al. 2014).

The seismic profile AA' spans 28 km, capturing the southern CB (Fig. 4). The section trends NW–SE, parallel to the axis of the CB. The profile reveals a symmetrical horst–graben structure delimited by two high-angle cross-basin faults, resulting in a topographic step of 0.40 s of TWTT, which is ~ 300 m. These faults created sufficient subsidence for 0.73 s (~ 550 m) of syn-tectonic sequences (Fig. 4). Siliciclastic material appears derived from uplifted areas surrounding the sub-basin and transport systems primarily located at the NW and SE ends of the CB (Fig. 3). The basal seismic facies is interpreted as highly fractured oceanic basement, observed as sigmoidal semi-continuous seismic reflections at a depth of 3.73 s on the southeastern graben flank. The lack of evidence of an active spreading center suggests the southern CB may be an abandoned axial graben. High-amplitude tabular reflections at a depth of 4.15 s indicate the location of the ancient spreading center, accompanied by magmatic intrusions forming sills, causing folding of the upper sedimentary sequences (Fig. 4).

The acoustic basement is fully exposed toward the northwest, while the southwestern footwall block is covered by 0.40 s (~ 300 m) of sediments. In the right-hand part of the seismic section (Fig. 4), the strata sequence of the uplifted footwall dips southeast, while the hanging wall slightly dips northwest, onlapping the bounding normal faults. Two sedimentary facies lie unconformably on the acoustic basement. The basal facies 0.33 s thick exhibits low-amplitude chaotic reflections, indicating low-energy sedimentation. Growth strata changes up-section to a seismic facies 0.40 s thick with good coherence and high-amplitude continuous reflections, indicating medium–high energy sedimentation environments (Fig. 4).

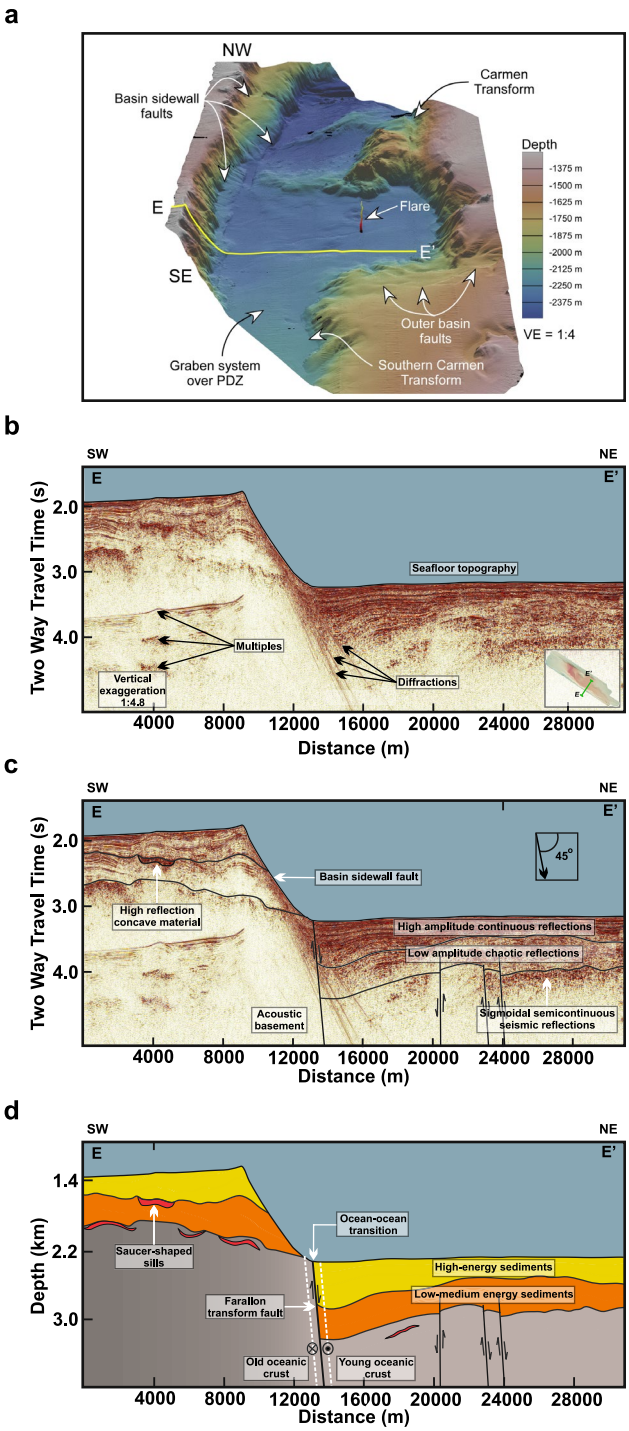

Fig. 8 Seismic profile E–E' spans the axial graben of the southern Carmen basin (SCB). **a** Perspective 3D view of the 40-m resolution bathymetry of the SCB, generated in Canvas Xgeo (https://www.canvasgfx.com). PDZ = principal displacement zone; VE = vertical exaggeration. The flare emerging from the seafloor was imaged using the Interactive Visualization Systems (IVS) Fledermaus 8.4.2 software package (www.qps.nl). **b** Raw seismic image. **c** Structural and stratigraphic seismic interpretation. **d** Interpreted geologic cross section. The seismic data reveal a steeply dipping Farallon transform fault (Fig. 3), which accommodates 0.73 s of syn-tectonic sedimentation. Toward the basin center, sedimentation decreases to 0.67 s thick (Fig. 4). Notably, an uplifted footwall exhibits a tabular-shaped high-amplitude seismic feature spanning ~ 2 km. This feature is interpreted as a saucer-shaped sill magmatic layer, leading to folding structures within the upper stratigraphic successions (Kluesner 2011)

Profile BB' spans 20 km across the central CB (Fig. 5). This sub-basin reveals an asymmetrical half-graben structure with a domino fault system defining the southern flank. The acoustic basement displays high-amplitude sigmoidal semi-continuous reflections at a depth of 3.73 s (~ 2800 m) and on both flanks at a depth of 3.20 s (~ 2400 m). In this basal seismic facies, the curvy reflections are interpreted as young oceanic crust of volcanic origin (Fig. 5), correlating with the basement rocks of the southern CB, located further southeast (Figs. 3 and 4). In the middle of the central CB, at a depth of 3.73 s (~ 2800 mbsl), a 1 km wide block of highly reflective material stands above the well-defined basement. The seismic expression of this feature resembles the ropey textured reflections seen in the surrounding basement, but it appears much brighter, which we interpret as the axis of an extinct seafloor spreading system that was active before the deposition of the overlying sedimentary sequence (Fig. 5).

Above the acoustic basement, there is a syn-tectonic sedimentary package composed of two seismic facies, reaching a thickness of ~ 300 m (Fig. 5). The underlying facies display layers with low-amplitude reflections and chaotic coherence, indicating sedimentation in low-energy environments. Along the NW margin, the basal sedimentary package shows a pronounced tilt toward the SE (Fig. 5). The overlying facies exhibit high-amplitude reflections with good lateral coherence, indicating sedimentation in medium to high-energy environments, similar to the southern CB (Fig. 4).

Profile CC' crosses the northern CB, spanning 17 km (Fig. 6), representing the deepest and narrowest sub-basin. The axial graben is defined by inward-stepping normal faults striking perpendicular to the principal displacement zone (Fig. 3), with a throw of 0.27 s along the graben margins. Our interpretation suggests these faults acted as fissures, accommodating the opening, and ~ 2400 m of young oceanic basement accreted between these fissure walls at a depth of 3.87 s (~ 2900 mbsl). This inner graben represents the active spreading axis of the CB. In this area, the high-amplitude tabular reflections represent basaltic rocks collected by the Woods Hole Oceanographic Institution, during the 2008 ROCA 9J-10 dive, using the (ROV) *Jason* aboard the R/V Atlantis. The sedimentary fill in the northern CB is notably thinner compared to the other Carmen sub-basins, measuring a thickness of 0.24 s (180 m). Observe, there is no sedimentary cover on top of the oceanic basement along the graben in the middle of the basin at a depth of 3.87 s (Fig. 6). The two sedimentary seismic facies, characterized by high- and

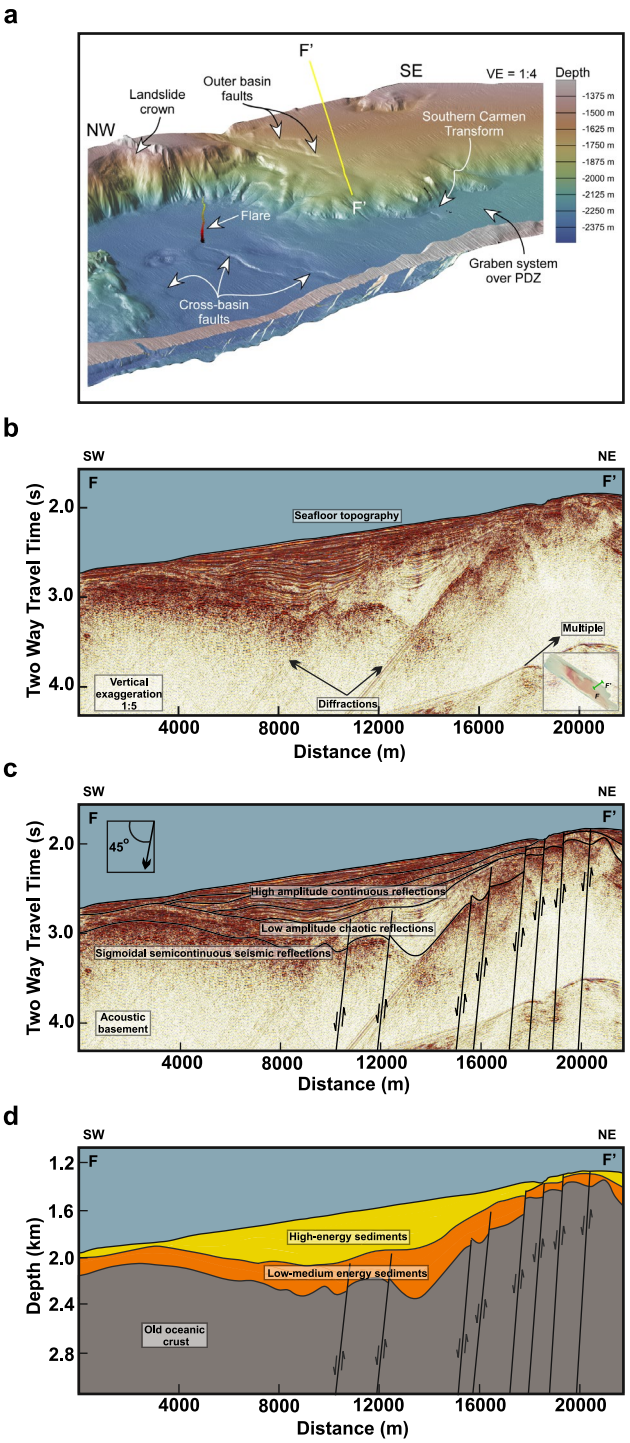

Fig. 9 Seismic profile F–F' illustrates the eastern part of the southern Carmen basin (SCB). **a** Perspective 3D view of the 40-m resolution bathymetry of the SCB, generated in Canvas Xgeo (https://www.canvasgfx.com). The flare emerging from the seafloor was imaged using the Interactive Visualization Systems (IVS) Fledermaus 8.4.2 software package (www.qps.nl). **b** Raw seismic image. **c** Structural and stratigraphic seismic interpretation. **d** Interpreted geologic cross section. The image displays a domino faulting system striking to the SE, accommodating 1.1 s of syn-tectonic strata at the depocenter. In (b) and (c), the sedimentary pattern reveals distinct seismic facies with inclined cross-bedding and erosion surfaces indicating southeastward deposition. These sedimentary packages potentially represent different facies compared to the sedimentary fills of the Carmen sub-basins, suggesting the presence of submarine fan deposits

low-amplitude reflection, are correlated on both flanks of the sub-basin and are dissected by the graben (Fig. 6). On the southeastern flank of the axial graben, the sigmoidal semi-continuous reflections reach the seafloor topography at a depth of 3.4 s depth, suggesting the young oceanic crust outcrops, whereas on the northwestern flank of the axial graben, the oceanic basement is covered by the two sedimentary units that we have interpreted throughout the CB.

Profile DD' spans ~ 43 km, overlapping ~ 5.7 km with the seismic profile CC', capturing the northern CB (Fig. 7). The seismic image reveals a sloped architecture controlled by a domino normal fault system striking southeast. Beneath the sedimentary cover, well-defined, high-amplitude sigmoidal semi-continuous reflections with a thickness of 0.27 s indicate the presence of an oceanic basement along the entire image (Fig. 7). Toward the SE, a transition zone is interpreted from two main features: (1) a change in the dip of the ropey layer (i.e., tilted to the right of the seismic image and horizontal to the left), and (2) a change in depth of the basement layer (i.e., 3.1 s depth to the right of the seismic image and 2.27 s depth to the left). This variation in bathymetric relief suggests a contrast in crustal density and across master transforms controlling adjacent basins (Fig. 3). The transition zone likely corresponds to a shift from younger oceanic crust in the northern Carmen sub-basin toward the SE to older oceanic crust adjacent to the Guaymas basin (Fig. 7). This area stands out for its abrupt seabed morphology, characterized by shallow chaotic reflections and acoustic signal loss, interpreted as uplifted and faulted sediments. This manifestation of off-axis magmatism is attributed to a dense network of sill intrusions throughout the surrounding areas (Teske et al. 2020). The latter interpretation is supported by the observation of off-transform volcanoes located in the northwestern part of the seismic profile, where the bathymetry is quite irregular, with small depressions and peaks reaching a zone of ~ 5200 m in length (Fig. 7).

Profile EE' extends 30 km and provides detailed information on the structure of the western region of the southern CB (Fig. 8). The seismic section intersects the Farallon transform fault toward the SW, interpreted as the basin's sidewall. At the hanging wall, the seismic facies sequence of this profile is consistent with the seismic profile AA', where the acoustic basement displays a prominent sigmoidal reflection of high-amplitude at a depth of 3.9 s (~ 2900 m), underlain by two distinct seismic facies characterized by low-amplitude non-coherence reflections, spanning a thickness of 0.33 s, and high-amplitude continuous reflections with a thickness of 0.4 s toward the uppermost part of the

sedimentary sequence (Figs. 4 and 8). Note that the footwall of the Farallon transform fault in the SW of the seismic image displays concave high-reflection features at depths of 2.24 and 2.59 s of TWTT (Fig. 8), suggesting the presence of saucer-shaped sill intrusions (Polteau et al. 2008; Kluesner 2011). The shallow sills in this area push the overlying sediments, forming forced folds. The dim area observed across the middle seismic facies may suggest fluid saturation due to lateral migration within the sedimentary cover (Fig. 8; Kluesner 2011). Additionally, the shallow sills in the footwall block indicate an oceanic basement of different composition, whereas the Farallon transform fault represents a transition zone, similar to the one observed in seismic profile DD' (Fig. 7), where we mark the transition between younger oceanic crust toward the southern CB to older oceanic crust adjacent to the continental shelf of the Baja California peninsula (Figs. 1, 2, 3 and 8).

Profile FF' is a 22 km long seismic profile that crosses the southeastern part of the southern CB (Fig. 9). It is anticipated that this profile would capture the southeastern extension of the Carmen transform fault. However, the identification of the bounding fault in this area is challenging and it is unlikely to extend this far to the SE. In map view, the Carmen transform fault bends strongly to the S, forming a releasing bend and splays into a series of normal faults dipping NW that control the SE margin of the southern CB (Fig. 3). These faults splay then bend again and become the Southern Carmen fault (Fig. 3). Moreover, the overlying seismic stratigraphy in the profile of Fig. 9 differs from previous interpretations in other portions of the CB. Here, the seismic stratigraphy is characterized by high-amplitude and laterally continuity reflectors, with cross-bedding structures, indicative of a submarine Gilbert-type fan delta depositional environment (Dorsey et al. 1995).

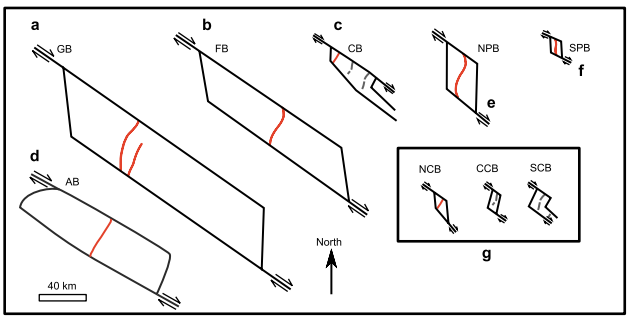

Fig. 10 Geometry models of southern basins in the Gulf of California. **a** Guaymas basin (GB). **b** Farallon basin (FB). **c** Carmen basin (CB). **d** Alarcon basin (CB). **e** Northern Pescadero basin (NPB). **f** Southern Pescadero basin (SPB). **g** Northern, Central, and southern sub-basins of the CB. The smaller structures, like the northern CB and NPB, exhibit a rhomboidal geometry, while the larger structures, such as GB and FB, display a rectangular geometry

Discussion

Geometry and timing of rifting in the Carmen basin

We conducted a comparative analysis between the CB geometry (Fig. 3), analog models of pull-apart basins (van Wijk et al. 2017; Wu et al. 2009), and neighboring structures in the southern GC (Fig. 10). A first-order observation from Fig. 3 is that the CB exhibits a basin morphology controlled by bounding master strike-slip transform fault with a length-to-width ratio of 5:1 According to Mann et al. (1983), rhomboidal-shaped pull-apart basins result from advanced stretching stages, which is more consistent with our observations from the map view analysis presented in Fig. 3. Length-to-width ratios increase by this process because the basin width remains fixed, while the extension increases by the offset of the releasing bend.

Comparing the geometry of the CB (Fig. 3) with the neighboring Guaymas and Farallon basins (Fig. 10A–C), we observe the latter two basins have a rectangular geometry, indicating a higher degree of deformation compared to the rhomboidal geometry of the CB (Fig. 3; Mann et al. 1983). However, when we compare the geometry of the sub-basins within the CB individually (Fig. 10D) with the less evolved Pescadero basin complex (Fig. 10E–F; Wu et al. 2009; Ramírez-Zerpa et al. 2022), we find that these basins share similar elongated rhomboidal structures with multiple depocenters separated by an intra-basinal highs (Wu et al. 2009; Ramírez-Zerpa et al. 2022; Fig. 3). It is worth noting that the boundaries depicted in Fig. 10 are speculative and based on limits proposed by multiple authors (Fletcher et al. 2007; Duque-Trujillo et al. 2015; Ferrari et al. 2018; Ramírez-Zerpa et al. 2022). Nevertheless, they provide a reasonable approximation of the geometry for each basin in the southern GC. Similar basin morphologies, such as those observed in the CB and the Pescadero basin complex

Table 1 Basin age inferred from length of ocean floor in the southern Gulf of California assuming a spreading rate of 52 mm/year (DeMets and Dixon 1999)

Name of the basin	Age (Ma)	Length (km)
Guaymas	6.1	320
Farallon	4.2	220
Alarcon	3.6	187
Carmen	1.9	100
Northern Pescadero	1.3	70
Southern Pescadero	0.5	25
Northern Carmen	0.4	20
Northern Carmen	0.4	20
Southern Carmen	0.4	20

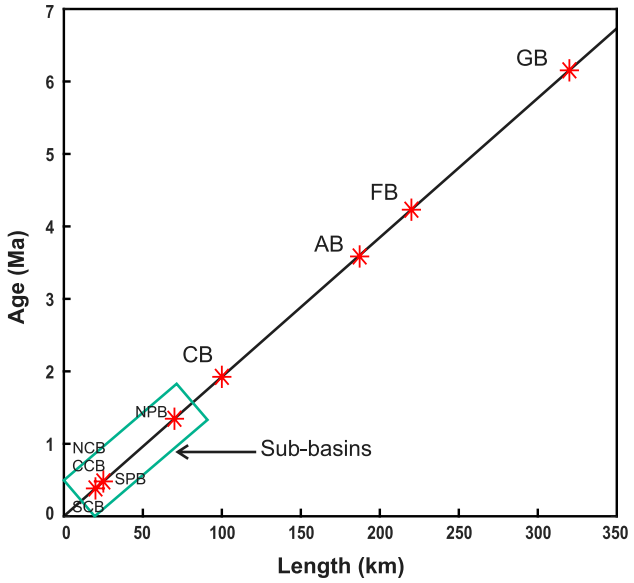

Fig. 11 Plot displaying the relationship between the onset of seafloor spreading and the length of the ocean floor in different pull-apart basins within the southern Gulf of California (Lizarralde et al. 2007; DeMets et al. 2010; Umhoefer 2011). The plot clearly shows that the time scales linearly with the size of the basin (Table 1). GB = Guaymas basin; FB = Farallon basin; CB = Carmen basin; NPB = Northern Pescadero basin; SPB = Southern Pescadero basin; NCB = Northern Carmen basin; CCB = Central Carmen basin; SCB = Southern Carmen basin

(Ramírez-Zerpa et al. 2022), can also be found in the northern GC basins (Farangitakis et al. 2021), the Vienna basin in Austria, and the Gulf of Eilat in the Red Sea (Wu et al. 2009), where the majority of transtensional deformation occurs along the principal displacement zones.

We now proceed to discuss a simple analysis of the amount of oceanic crust created along the southern GC basins can be derived using basic plate kinematics in relation to the onset of oceanic accretion, assuming a typical spreading rate of 52 mm/year (Table 1; Figs. 10 and 11; DeMets and Dixon 1999). Basin length is a function of stretching related to strike-slip displacement, and increased displacement leads to an expansion in the width of the fault zone, resulting in broader structures (Gürbüz 2010). As expected, the larger oceanic basins, such as the Guaymas and Farallon basins, are older than the smaller ones, including the northern CB, central CB, southern CB sub-basins, and the Pescadero basin complex (Fig. 11). The Guaymas basin exhibits a length-to-width ratio of ~ 5:1, with a length of ~ 320 km and a width of ~ 65 km. In contrast, the Farallon basin has a length-to-width ratio of 4:1, with a length of ~ 220 km and a width of ~ 55 km. The Alarcon basin, on the other hand, shows a similar ratio of ~ 4:1, with a length of ~ 187 km, and a width of ~ 50 km. The length-to-width ratios reported in this work are in good agreement with those reported by Lonsdale (1989). However, they differ slightly from the accretionary oceanic crust lengths reported for the Guaymas (280 km) and Alarcón (135 km) basins by Lizarralde et al. (2007). This deviation may result from a transitional zone between oceanic and continental crust, which appears to be somewhat diffuse. These basins are considered the oldest basins of the entire southern GC, with a timing of rifting between 3.6 and 6.1 Ma (Table 1; Kluesner et al. 2014). In contrast, the northern CB, central CB, southern CB sub-basins, and the Pescadero basin complex have length-to-width ratios of ~ 1:1, with lengths and widths both ~ 20 km, whereas the axial graben further SW of the southern CB has a length-to-width ratio of ~ 2:1 (not included in Figs. 10 and 11). These sub-basins are regarded as the youngest basins in the southern GC, with ages ranging from 0.4 to 1.3 Ma. In the case of the CB, each sub-basin took 400 Ka to form, while the CB as a whole presents an age of 1.9 Ma (Table 1). Thus, the low length-to-width ratios observed in the CB suggest that these sub-basins are short-lived features within rapidly evolving strike–slip zones (Mann et al. 1983). According to Ferrari et al. (2018), the intra-basin highs (Figs. 3 and 5) and the transform fault volcanism (Figs. 3, and 7) observed in the CB are interpreted as early Pleistocene seamounts. This interpretation is in good agreement with our estimated timing of faulting and basin formation derived from our analysis in Figs. 10, 11, and Table 1.

Moreover, to understand the geologic evolution of the CB, it is also valuable to compare its spreading system with the neighboring Guaymas and Farallon systems. The spreading axes of these systems are wider (2–3 times) than the narrow width (20 km) of the CB (Figs. 1, 2, 3). Additionally, the adjacent spreading systems have significantly more accreted oceanic crust (320 and 220 km) compared to the CB's 100 km (Table 1). Therefore, for several million years before the existence of the CB, the Guaymas and Farallon spreading systems must have been connected by a segment of the plate margin that was dominated by transform faulting. Based on these relationships, we propose that the CB was created at 1.9 Ma within this transform environment.

Crustal lithology and the transition from old to young oceanic crust

In this section, we analyze the lithological composition of the CB basement based on the seismic interpretation derived from Figs. 4, 5, 6, 7, 8, 9. We further discuss the basin's boundaries to distinguish between old and young oceanic crust and the transition between continental and ocean basement (Fig. 12). Our seismic interpretation suggests the CB acoustic basement is composed of highly reflective ropey layers with good lateral continuity, similar to those found in neighboring basins. These layers have been identified as basaltic lava flows and intruded sills

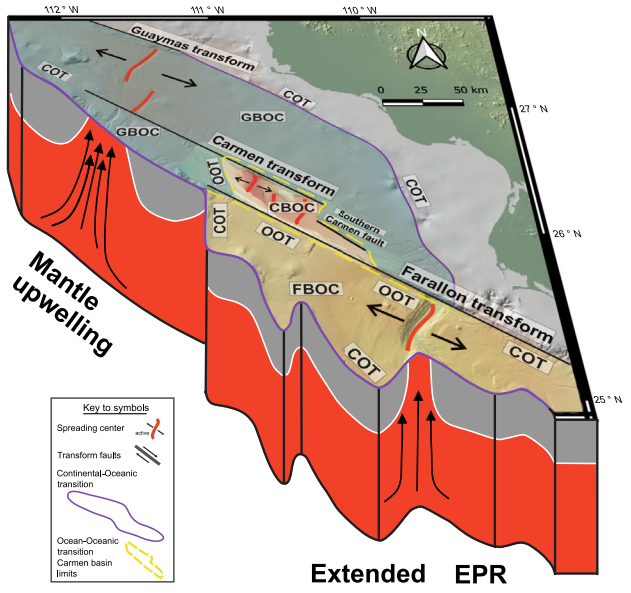

Fig. 12 Regional map illustrating the crustal boundaries of the Guaymas, Carmen, and Farallon basins. The oceanic crust of the Guaymas basin is highlighted in light green, while the CB is represented by the bathymetric data from the multi-beam survey (40-m resolution; Fig. 3). The Farallon basin is highlighted in light yellow. The dotted yellow line indicates the transition from old oceanic crust (late Miocene for the Guaymas basin and early Pliocene for the Farallon basin; Lizarralde et al. 2007; DeMets et al. 2010; Umhoefer 2011) to young oceanic crust (early Pleistocene for the Carmen basin; Table 1). The purple line marks the boundary between continental and oceanic crust. CBOC = Carmen basin oceanic crust; COT = Continental–oceanic transition; FBOC = Farallon basin oceanic crust; GBOC = Guaymas basin oceanic crust; OOT = Oceanic–oceanic transition. The schematic cross-section model is based on interpretations by Gregg et al. (2007), Wang et al. (2009) and Di Luccio et al. (2014). The cartoon depicts the dynamic upwelling of the mantle at the mouth of the Gulf of California as an extension of the East Pacific Rise (EPR), which facilitates the formation of new oceanic floor

within sedimentary deposits, as found in collected rocks in the axial graben of the northern Carmen basin (Fig. 6), and adjacent Farallon and Guaymas basins (Piñero-Lajas 2008; Lizarralde et al. 2007; Kluesner 2011). The basement rocks outcrop widely along the three sub-basins of the CB, the spreading center, and the structural highs, forming at least ~ 80 km of newly formed oceanic crust (Figs. 4–7). In Fig. 12, we identify three distinct segments of oceanic crust according to their estimated formation age (Figs. 10, 11, and Table 1). Two things are noteworthy in Fig. 12. (i) The eastern transition between continental and oceanic crust is delimited at the Sonora and Sinaloa continental shelf border by a series of en-echelon scarps juxtaposing continental and oceanic crust (Figs. 1, 2, and 12). By contrast, the transition along the western and southwestern basin margins is defined by a series of rotated blocks within a low-angle faulting system along the Baja California continental shelf border, as revealed by previous studies (Bot et al. 2016; Macias-Iniguez et al. 2019). And (ii), the CB separates the Guaymas and Farallon basins through an oceanic–oceanic crustal boundary. Cross-cutting and structural relations indicate that the Carmen transform fault and Farallon transform fault bounding the CB are younger than the oceanic crust along the inner margins of the Guaymas and Farallon basins (Figs. 10, 11 and Table 1).

According to Polteau et al. (2008), saucer-shaped intrusions form when a buoyant sheet of rising melt, driven by magmatic pressure from a magma source, exceeds the pressure exerted by the surrounding sediment. The seismic profiles across the CB reveal concave, high-reflection material interpreted as saucer-shaped igneous sills (Kluesner 2011). These magmatic intrusions have varying lengths but average diameters of 1–2 km (Fig. 8). They are associated with overburden deformations, fluid migration through faults, and potential feeder networks (Kluesner 2011; Negrete-Aranda et al. 2019, 2021; Sarkar et al. 2022; Figs. 4, 6, and 8). These shallow sills are observed within a young oceanic crust, representing sites of magmatic crustal accretion in the actively growing basin (Figs. 4 and 6). Kluesner et al. (2011) reported that the sill located southwest of Farallon Transform spans a length of 2 km, with a thickness of 280 m, and features sharply upturned tips buried ~ 340 m of sediments (Fig. 8). Formation of sediment-sill complexes, which involve the intercalations of igneous sills and sedimentary rocks, has been observed in both the central Guaymas basin and southern Farallon basin (Piñero-Lajas 2008; Kluesner 2011; Lizarralde et al. 2011; Sarkar et al. 2022). Thus, Kluesner (2011) suggests that the geometry of sills in the Gulf of California, as derived through finite element modeling, is predominantly influenced by factors such as the depth of emplacement, displacement, and deformation of the overlying strata.

Kinematics of transform faults and spreading center instabilities in the Carmen basin

In the southern GC, cross-cutting relations suggest that the formation of the CB occurred after seafloor spreading initiated in the Farallon and Guaymas basins. Kinematic instability of the bounding faults led to the propagation of the Carmen transform fault and the Farallon transform fault, eventually forming the CB (Fig. 10, 12, and Table 1). A possible mechanism determining the stability of this family of boundaries is the pooling of erupted lavas observed in topographic lows within the transform fault domain (e.g., Carmen transform fault; Fig. 3). According to Gregg et al. (2007), this *leaky* magmatic accretion results from the presence of intermediate-fast-slipping transform faults, a configuration frequently observed at the East Pacific Rise, where basaltic lavas indicate crustal accretion within the transform

fault region, as seen in the Garret and Siqueiros transform faults. Gregg et al. (2006, 2007) also suggest that an intra-transform spreading center is a series of fault lines offset by short ridges. These features facilitate active seafloor spreading, resulting in crustal accretion.

In the case of the CB, our proposed model in Fig. 12 is consistent with the interpretations by Gregg et al. (2007), Wang et al. (2009), and Di Luccio et al. (2014). According to this model, the fast rifting in the southern GC is driven by mantle upwelling, leading to the formation of new oceanic spreading centers connected by intermediate-fast slipping transform faults, including the Carmen transform fault and the Farallon transform fault (Fig. 3). These observations align with the cross-sectional features presented in Fig. 12, which depict the extended East Pacific Rise, as well as mantle upwelling patterns similar to those found in tomography studies by Wang et al. (2009), Zhao (2004), Di Lluccio (2014). According to Wang et al. (2009), the current configuration of the main spreading center system in the Wagner, Delfin, and Guaymas basins is influenced by partially melted mantle pockets spaced ~ 250 km apart. Furthermore, Di Luccio et al. (2014) have observed slow anomaly asthenosphere upwelling beneath the Pescadero basin and Alarcon basin in the southern GC.

To explain the development of the CB, we also follow the model proposed by Sims et al. (1999). The idea is that transform faults can evolve from strike-slip to normal-oblique, creating a network of sub-basins above a thin, ductile basal décollement. The domino faulting system observed toward the northern CB (Figs. 2 and 7) suggests the presence of a SW-directed detachment surface. This configuration allows magma intrusion through crustal thinning and mantle upwelling, resulting in volcanic and intrusive features along the Farallon transform fault (Figs. 2 and 3; Kusznir and Karner 2007). This process may lead to the development of a hinge zone, northwest of the northern CB, near the structural high interpreted as a young mud volcano in Fig. 7, similar to the 20° N basin along the Owen Fracture Zone in the NW Indian Ocean (Rodriguez et al. 2013). These observations are also consistent with the wide distribution of east and west-directed low-angle normal faults along the GC (González-Fernández et al. 2005; Martín-Barajas et al. 2013; Macias-Iñiguez et al. 2019), where faults are believed to contribute to more efficient stretching and plastic rebound of the underlying lithospheric mantle, leading to the formation of metamorphic core complexes associated with regional rolling-hinge structures (Fletcher and Spelz 2009). Comparable structural systems can also be observed in bathymetric data of the Mid-Atlantic Ridge, where core complexes associated with basal detachments and normal faulting parallel to the ridge axis develop (Howell et al. 2019).

The CB consists of three spreading centers within the same plate-margin segment, indicating significant instability in the localization of the spreading process. These spreading centers form sub-basins with increasingly advanced pull-apart geometries from south to north (Figs. 4, 5, and 6). Lithospheric strength plays a crucial role in strain localization, and compositional and thermal heterogeneities in the upper mantle are likely to have significantly influenced the positioning of spreading axes. Seismic tomography conducted by Wang et al. (2009) and Di Luccio et al. (2014) revealed areas of robust upwelling with low-shear velocity near the more stable Guaymas and Farallon spreading systems. However, it is worth noting that these mantle anomalies are offset toward the east compared to the surface trace of these spreading systems as shown in mantle tomography studies made by the same authors. Moreover, Fletcher et al. (2007) proposed that the anomalous upper mantle associated with the paleo East Pacific Rise, west of the Baja California microplate, likely continued to be overridden by western North America following the middle Miocene ridge–trench collision, which marked the onset of rifting in the proto-GC. This would explain why the centers of anomalous mantle are situated east of the Guaymas and Farallon spreading axes, suggesting that the passage of the CB over thermally and compositionally heterogeneous mantle could have contributed to the observed instabilities in strain localization. The middle Miocene ridge–trench collision was also accompanied by the opening of a deep slab window beneath the proto-GC (Fletcher et al. 2007), generating additional compositional and thermal anomalies in the upper mantle.

Another factor that strongly controls strain localization is the distribution of applied tectonic loads along the plate margin. Fletcher et al. (2007) proposed that the Baja California microplate, along with its underplated Farallon-derived microplates, became welded to the Pacific plate across the paleo East Pacific Rise. Consequently, the asthenospheric window beneath the GC continues to widen due to the northwestward drift of the Pacific plate along the trailing edge of the western limit of the Baja California microplate, which has been shown by Di Luiccio et al. (2014) to coincide with the western limit of the Farallon slab at depth. Thus, the northwest migration of the spreading axes that we have documented in the CB may be a function of the northwest migration of applied tectonic loads.

Conclusions

By examining the seafloor morphology and the seismic structure at depth of the CB, we gain insights into the deformation process at a small scale. The development of three sub-basins with contrasting morphologies suggests progressive strain from the southern CB toward the northern CB, where the current spreading center is located. This pattern indicates that the sub-basin system formed at

different geologic times due to rapid extension, resulting in the abandonment of the southern sub-basins and the establishment of the current spreading center in the northern sub-basin. Our findings also suggest an estimated age of ~ 1.9 Ma, indicating that, despite being a young structure, the basin has reached a level of maturity similar to those found in oceanic basins. Furthermore, based on our comparative geometric analysis with analog models and other natural examples of pull-apart basins, we propose that the CB is a product of transtensional deformation rather than pure strike-slip extension.

Despite variations in the predicted degree of basin evolution according to different models, the current stage of the CB appears to mark the transition between crustal thinning and the eventual oceanic crust rupture, creating spreading centers and generating new oceanic crust. The seismic interpretation reveals an acoustic basement consisting of volcanic rocks, indicating the development of a new oceanic floor across the CB. Variations in basin bathymetry suggest the juxtaposition of different materials, with structural highs representing either a crystalline basement or indicating late Miocene-to-early Pleistocene volcanic activity. The oceanic crust of the CB is bounded by major basin sidewall faults, exhibiting magmatic activity along the transform faults connecting the Guaymas and Farallon basin oceanic crusts. This magmatic accretion indicates intermediate-fast-slipping fault propagation separated by a segment of intra-transform spreading center, resembling the extensional dynamics of the East Pacific Rise toward the mouth of the GC.

Depositional relations and cross-cutting correlations in the seismic stratigraphy indicate that CB formation began in the southern CB. Sediment thickness decreases systematically from the southern CB to the northern CB, indicating strain localization and spreading center instabilities within the CB. The extended East Pacific Rise beneath the GC influences the relocation of spreading axes, favoring areas with thinner, fractured crust. This kinematic setting explains the sequential abandonment of sub-basins and their fossil spreading centers in the southern and central CB, ultimately leading to the active spreading center in the northern CB. Further north, near the active volcanism of the Carmen transform fault, the development of mud volcanoes could drive the migration of a future spreading center.

Supplementary Information The online version contains supplementary material available at https://doi.org/10.1007/s00531-024-02426-6.

Acknowledgements This research was supported by CONAHCYT, providing scholarship No. 1011828 to Marc Julià Miralles for his Ph.D. project. Funding was also received from CONAHCYT project No. 319430 awarded to Ismael Yarbuh, and UABC project No. 401/1/C/13/23 awarded to Ronald M. Spelz. We thank the Schmidt Ocean Institute and the R/V *Falkor* crew, especially Lead Tech John Fulmer, MTs Veit Huehnerbach, and Kaarel Kaspar Rais, for their support during expedition FK210922. Our gratitude goes to Isabela Macias and Juan Manuel Wagner for their contributions to seismic and illustration software management. We are also grateful to Jared Kluesner and the anonymous reviewer for their valuable suggestions that improved the manuscript. This work is contribution No. 7 from the academic team *Geología Costera UABC-CA-38*.

Data availability The seismic data utilized in this study is accessible online through an institutional repository hosted at http://cicese.repositorioinstitucional.mx/jspui/handle/1007/3659. Additionally, the bathymetry data is readily available via the GeoMappApp database (http://www.geomapapp.org), which is administered by the Lamont-Doherty Earth Observatory of Columbia University. Both resources allow unrestricted access to the data, enabling users to retrieve and utilize the information for detailed observations or future analyses.

Declarations

Conflict of interest The authors declare no conflict of interest.

Open Access This article is licensed under a Creative Commons Attribution 4.0 International License, which permits use, sharing, adaptation, distribution and reproduction in any medium or format, as long as you give appropriate credit to the original author(s) and the source, provide a link to the Creative Commons licence, and indicate if changes were made. The images or other third party material in this article are included in the article's Creative Commons licence, unless indicated otherwise in a credit line to the material. If material is not included in the article's Creative Commons licence and your intended use is not permitted by statutory regulation or exceeds the permitted use, you will need to obtain permission directly from the copyright holder. To view a copy of this licence, visit http://creativecommons.org/licenses/by/4.0/.

References

Aragón-Arreola M, Martín-Barajas A (2007) Westward migration of extension in the northern Gulf of California Mexico. Geology 35(6):571–574. https://doi.org/10.1130/G23360A.1

Aragón-Arreola M, Morandi M, Martín-Barajas A, Delgado-Argote L, González-Fernández A (2005) Structure of the rift basins in the central Gulf of California: kinematic implications for oblique rifting. Tectonophysics 409(1–4):19–38. https://doi.org/10.1016/j.tecto.2005.08.002

Atwater T (1970) Implications of plate tectonics for the Cenozoic tectonic evolution of western North America. Geol Soc Am Bull 81(12):3513–3536. https://doi.org/10.1130/0016-7606(1970)81[3513:IOPTFT]2.0.CO;2

Atwater T (1989) Plate tectonic history of the northeast Pacific and western North America. The Eastern Pacific Ocean and Hawaii Geology of North America. Geological Society of America, Boulder, pp 21–72. https://doi.org/10.1130/DNAG-GNA-N.21

Atwater T, Stock J (1998) Pacific-North America plate tectonics of the Neogene southwestern United States: an update. Int Geol Rev 40(5):375–402. https://doi.org/10.1080/00206819809465216

Balestrieri ML, Ferrari L, Bonini M, Duque-Trujillo J, Cerca M, Moratti G, Corti G (2017) Onshore and offshore apatite fission-track dating from the southern Gulf of California: insights into the time-space evolution of the rifting. Tectonophysics 719:148–161. https://doi.org/10.1016/j.tecto.2017.05.012

Bennett SE, Oskin ME, Iriondo A, Kunk MJ (2016) Slip history of the La Cruz fault: development of a late Miocene transform in response to increased rift obliquity in the northern Gulf of

California. Tectonophysics 693:409–435. https://doi.org/10.1016/j.tecto.2016.06.013
Bohannon RG, Parsons T (1995) Tectonic implications of post–30 Ma Pacific and North American relative plate motions. Geol Soc Am Bull 107(8):937–959. https://doi.org/10.1130/0016-7606(1995)107%3C0937:TIOPMP%3E2.3.CO;2
Bot A, Geoffroy L, Authemayou C, Bellon H, Graindorge D, Pik R (2016) Miocene detachment faulting predating EPR propagation: Southern Baja California. Tectonics 35(5):1153–1176. https://doi.org/10.1002/2015TC004030
Buck WR (1988) Flexural rotation of normal faults. Tectonics 7(5):959–973. https://doi.org/10.1029/TC007i005p00959
Buck WR (1993) Effect of lithospheric thickness on the formation of high-and low-angle normal faults. Geology 21(10):933–936. https://doi.org/10.1130/0091-7613(1993)021%3C0933:EOLTOT%3E2.3.CO;2
Bunge HP, Grand SP (2000) Mesozoic plate-motion history below the northeast Pacific Ocean from seismic images of the subducted Farallon slab. Nature 405(6784):337–340. https://doi.org/10.1038/35012586
Chopra S, Marfurt KJ (2007) Seismic attributes for prospect identification and reservoir characterization. Society of Exploration Geophysicists and European Association of Geoscientists and Engineers, Tulsa, p 457. https://doi.org/10.1190/1.9781560801900
Christie-Blick N, Biddle KT (1985) Deformation and basin formation along strike-slip faults. SEPM Spec Publ 37:1–34. https://doi.org/10.2110/pec.85.37.0001
Contreras-Pérez J, Ramírez-Zerpa N, Negrete-Aranda R (2012) Modelos tectonoestratigráficos de las cuencas de Tiburón y Wagner en el norte del Golfo de California. Revista Mexicana De Ciencias Geológicas 29(1):140–157
DeMets C, Dixon TH (1999) New kinematic models for Pacific-North America motion from 3 Ma to present, I: evidence for steady motion and biases in the NUVEL-1A model. Geophys Res Lett 26(13):1921–1924. https://doi.org/10.1029/1999GL900405
DeMets C, Gordon RG, Argus DF (2010) Geologically current plate motions. Geophys J Int 181(1):1–80. https://doi.org/10.1111/j.1365-246X.2009.04491.x
Di Luccio F, Persaud P, Clayton RW (2014) Seismic structure beneath the Gulf of California: a contribution from group velocity measurements. Geophys J Int 199(3):1861–1877. https://doi.org/10.1093/gji/ggu338
Dorsey RJ, Umhoefer PJ, Renne PR (1995) Rapid subsidence and stacked Gilbert-type fan deltas, Pliocene Loreto basin, Baja California Sur Mexico. Sediment Geol 98(1–4):181–204. https://doi.org/10.1016/0037-0738(95)00032-4
Duque-Trujillo J, Ferrari L, Norini G, López-Martínez M (2014) Miocene faulting in the southwestern Sierra Madre Occidental, Nayarit, Mexico: kinematics and segmentation during the initial rifting of the southern Gulf of California. Revista Mexicana De Ciencias Geológicas 31(3):283–302
Duque-Trujillo J, Ferrari L, Orozco-Esquivel T, López-Martínez M, Lonsdale P, Bryan SE, Kluesner J, Piñero-Lajas D, Solari L (2015) Timing of rifting in the southern Gulf of California and its conjugate margins: insights from the plutonic record. Geol Soc Am Bull 127(5–6):702–736. https://doi.org/10.1130/B31008.1
Farangitakis GP, McCaffrey KJ, Willingshofer E, Allen MB, Kalnins LM, van Hunen J, Persaud P, Sokoutis D (2021) The structural evolution of pull-apart basins in response to changes in plate motion. Basin Res 33(2):1603–1625. https://doi.org/10.1111/bre.12528
Ferrari L, Orozco-Esquivel T, Bryan SE, Lopez-Martinez M, Silva-Fragoso A (2018) Cenozoic magmatism and extension in western Mexico: Linking the Sierra Madre Occidental silicic large igneous province and the Comondú Group with the Gulf of California rift. Earth Sci Rev 183:115–152. https://doi.org/10.1016/j.earscirev.2017.04.006
Fletcher JM, Munguia L (2000) Active continental rifting in southern Baja California, Mexico: implications for plate motion partitioning and the transition to seafloor spreading in the Gulf of California. Tectonics 19(6):1107–1123. https://doi.org/10.1029/1999TC001131
Fletcher JM, Spelz RM (2009) Patterns of Quaternary deformation and rupture propagation associated with an active low-angle normal fault, Laguna Salada, Mexico: evidence of a rolling hinge? Geosphere 5(4):385–407. https://doi.org/10.1130/GES00206.1
Fletcher JM, Kohn BP, Foster DA, Gleadow AJ (2000) Heterogeneous Neogene cooling and exhumation of the Los Cabos block, southern Baja California: evidence from fission-track thermochronology. Geology 28(2):107–110. https://doi.org/10.1130/0091-7613(2000)28%3C107:HNCAEO%3E2.0.CO;2
Fletcher JM, Pérez-Venzor JA, González-Barba G, Aranda-Gomez JJ (2003) Ridge-trench interactions and the ongoing capture of the Baja California microplate—New from the southern Gulf extensional province. Geologic transects across the Cordilleran Mexico, Guidebook for field trips of the 99th Annual meeting of the Cordilleran Section of the Geological Society of America, Volume Publicacion Especial 1: Mexico. Universidad Nacional Autónoma de México, Instituto de Geología, D.F., pp 13–31
Fletcher JM, Grove M, Kimbrough D, Lovera O, Gehrels GE (2007) Ridge-trench interactions and the Neogene tectonic evolution of the Magdalena shelf and southern Gulf of California: Insights from detrital zircon U–Pb ages from the Magdalena fan and adjacent areas. Geol Soc Am Bull 119(11–12):1313–1336. https://doi.org/10.1130/B26067.1
Fornari DJ, Gallo DG, Edwards MH, Madsen JA, Perfit MR, Shor AN (1989) Structure and topography of the Siqueiros transform fault system: evidence for the development of intra-transform spreading centers. Mar Geophys Res 11:263–299. https://doi.org/10.1007/BF00282579
González-Escobar M, Suárez-Vidal F, Hernández-Pérez JA, Martín-Barajas A (2010) Seismic reflection-based evidence of a transfer zone between the Wagner and Consag basins: implications for defining the structural geometry of the northern Gulf of California. Geo-Mar Lett 30(6):575–584. https://doi.org/10.1007/s00367-010-0204-0
González-Fernández A, Dañobeitia JJ, Delgado-Argote LA, Michaud F, Córdoba D, Bartolomé R (2005) Mode of extension and rifting history of upper Tiburón and upper Delfín basins, northern Gulf of California. J Geophys Res Solid Earth. https://doi.org/10.1029/2003JB002941
Gregg PM, Lin J, Smith DK (2006) Segmentation of transform systems on the East Pacific Rise: implications for earthquake processes at fast-slipping oceanic transform faults. Geology 34(4):289–292. https://doi.org/10.1130/G22212.1
Gregg PM, Lin J, Behn MD, Montési LG (2007) Spreading rate dependence of gravity anomalies along oceanic transform faults. Nature 448(7150):183–187. https://doi.org/10.1038/nature05962
Gürbüz A (2010) Geometric characteristics of pull-apart basins. Lithosphere 2(3):199–206. https://doi.org/10.1130/L36.1
Howell SM, Olive JA, Ito G, Behn MD, Escartin J, Kaus B (2019) Seafloor expression of oceanic detachment faulting reflects gradients in mid-ocean ridge magma supply. Earth Planet Sci Lett 516:176–189. https://doi.org/10.1016/j.epsl.2019.04.001
Kluesner JW (2011) Marine geophysical study of cyclic sedimentation and shallow sill intrusion in the floor of the Central Gulf of California. University of California, San Diego (Ph.D. Thesis, 231 pp). https://www.proquest.com/openview/10ac7f482ea0c51dbd43afd312e6e8fc/1?pq-origsite=gscholar&cbl=18750
Kluesner J, Lonsdale P, González-Fernández A (2014) Late Pleistocene cyclicity of sedimentation and spreading-center structure in the

Central Gulf of California. Mar Geol 347:58–68. https://doi.org/10.1016/j.margeo.2013.11.001

Kusznir NJ, Karner GD (2007) Continental lithospheric thinning and breakup in response to upwelling divergent mantle flow: application to the Woodlark, Newfoundland and Iberia margins. Geol Soc, Lond, Spec Publ 282(1):389–419. https://doi.org/10.1144/SP282.16

Lavier LL, Roger Buck W, Poliakov AN (1999) Self-consistent rolling-hinge model for the evolution of large-offset low-angle normal faults. Geology 27(12):1127–1130. https://doi.org/10.1130/0091-7613(1999)027%3C1127:SCRHMF%3E2.3.CO;2

Lizarralde D, Axen GJ, Brown HE, Fletcher JM, González-Fernández A, Harding AJ, Holbrook WS, Kent GM, Paramo P, Sutherland F, Umhoefer PJ (2007) Variation in styles of rifting in the Gulf of California. Nature 448(7152):466–469. https://doi.org/10.1038/nature06035

Lizarralde D, Soule SA, Seewald JS, Proskurowski G (2011) Carbon release by off-axis magmatism in a young sedimented spreading centre. Nat Geosci 4(1):50–54. https://doi.org/10.1038/ngeo1006

Lonsdale P (1989) Geology and tectonic history of the Gulf of California. In: Hussong D, Winterer EL, Decker RW (eds) The Eastern Pacific Ocean and Hawaii, The Geology of North America, N. Geological Society of America, Boulder, pp 499–521. https://doi.org/10.1130/dnag-gna-n.499

Macias-Iñiguez I, Yarbuh I, Spelz-Madero R, González-Fernández A, Fletcher JM, Contreras J, Ramírez-Zerpa N, Santa-Rosa-del-Río MA, Guardado-France R (2019) Modo de extensión de la corteza y formación del Sistema Extensional de Cerralvo, sur del Golfo de California, a partir de datos de reflexión sísmica en 2D. Revista Mexicana De Ciencias Geológicas 36(3):334–347. https://doi.org/10.22201/cgeo.20072902e.2019.3.1352

Mann P (2007) Global catalogue, classification and tectonic origins of restraining-and releasing bends on active and ancient strike-slip fault systems. Geol Soc, Lond, Spec Publ 290(1):13–142. https://doi.org/10.1144/sp290.2

Mann P, Hempton MR, Bradley DC, Burke K (1983) Development of pull-apart basins. J Geol 91(5):529–554. https://doi.org/10.1086/628803

Martín-Barajas A, González-Escobar M, Fletcher JM, Pacheco M, Oskin M, Dorsey R (2013) Thick deltaic sedimentation and detachment faulting delay the onset of continental rupture in the Northern Gulf of California: analysis of seismic reflection profiles. Tectonics 32(5):1294–1311. https://doi.org/10.1002/tect.20063

McKenzie D (1978) Active tectonics of the Alpine—Himalayan belt: the Aegean Sea and surrounding regions. Geophys J Int 55(1):217–254. https://doi.org/10.1111/j.1365-246X.1978.tb04759.x

Negrete-Aranda R, Contreras J, Spelz RM (2013) Viscous dissipation, slab melting, and post-subduction volcanism in south-central Baja California Mexico. Geosphere 9(6):1714–1728. https://doi.org/10.1130/GES00901.1

Negrete-Aranda R, Neumann F, Harris RN, Contreras J, Zierenberg RA, Caress DW (2019) First heat flow measurements in the Auka and JaichMaa'ja'ag vent fields Pescadero Basin, Southern Gulf of California. In: AGU Fall Meeting Abstracts Vol. 2019, pp V13D-0187. https://ui.adsabs.harvard.edu/abs/2019AGUFM.V13D0187N/abstract

Negrete-Aranda R, Neumann F, Contreras J, Harris RN, Spelz RM, Zierenberg R, Caress DW (2021) Transport of Heat by Hydrothermal Circulation in a Young Rift Setting: Observations from the Auka and JaichMaa ja' ag' vent Fields in the Pescadero Basin, Southern Gulf of California. J Geophys Res: Solid Earth 126(8):e2021JB022300. https://doi.org/10.1029/2021JB022300

Nicholson C, Sorlien CC, Atwater T, Crowell JC, Luyendyk BP (1994) Microplate capture, rotation of the western Transverse Ranges, and initiation of the San Andreas transform as a low-angle fault system. Geology 22(6):491–495. https://doi.org/10.1130/0091-7613(1994)022%3C0491:MCROTW%3E2.3.CO;2

Piñero-Lajas D (2008) Seismic reflection and 40Ar-39Ar dating of continental basement in the western margin of Farallon basin (southern Gulf of California, Mexico). CICESE, Ensenada, Baja California, México. M.Sc. thesis in Earth Science, p 155. https://biblioteca.cicese.mx/catalogo/tesis/ficha.php?id=17932

Pockalny RA, Fox PJ, Fornari DJ, Macdonald KC, Perfit MR (1997) Tectonic reconstruction of the Clipperton and Siqueiros Fracture Zones: evidence and consequences of plate motion change for the last 3 Myr. J Geophys Res: Solid Earth 102(B2):3167–3181. https://doi.org/10.1029/96JB03391

Polteau S, Ferré EC, Planke S, Neumann ER, Chevallier L (2008) How are saucer-shaped sills emplaced? Constraints from the Golden Valley Sill South Africa. J Geophys Res Solid Earth. https://doi.org/10.1029/2008JB005620

Ramírez-Zerpa N, Spelz RM, Yarbuh I, Negrete-Aranda R, Contreras J, Clague DA, Neumann F, Caress DW, Zierenberg RA, González-Fernández A (2022) Architecture and tectonostratigraphic evolution of the Pescadero Basin Complex, southern Gulf of California: analysis of high-resolution bathymetry data and seismic reflection profiles. J S Am Earth Sci. https://doi.org/10.1016/j.jsames.2021.103678

Rodriguez M, Chamot-Rooke N, Fournier M, Huchon P, Delescluse M (2013) Mode of opening of an oceanic pull-apart: The 20° N Basin along the Owen Fracture Zone (NW Indian Ocean). Tectonics 32(5):1343–1357. https://doi.org/10.1002/tect.20083

Sarkar S, Moser M, Berndt C, Doll M, Böttner C, Chi WC, Klaeschen D, Galerne C, Karstens J, Geilert S, Mortera-Gutierrez C, Hensen C (2022) Thermal state of the Guaymas Basin derived from gas hydrate bottom simulating reflections and heat flow measurements. J Geophys Res Solid Earth. https://doi.org/10.1029/2021JB023909

Sheriff RE, Geldart LP (1995) Exploration seismology volume I: history, theory and data acquisition. Cambridge University Press, Cambridge, p 559

Sims D, Ferrill DA, Stamatakos JA (1999) Role of a ductile decollement in the development of pull-apart basins: experimental results and natural examples. J Struct Geol 21(5):533–554. https://doi.org/10.1016/S0191-8141(99)00010-3

Spencer JE, Normark WR (1979) Tosco-Abreojos fault zone: a Neogene transform plate boundary within the Pacific margin of southern Baja California Mexico. Geology 7(11):554–557. https://doi.org/10.1130/0091-7613(1979)7%3C554:TFZANT%3E2.0.CO;2

Stock JM, Hodges KV (1989) Pre-Pliocene extension around the Gulf of California and the transfer of Baja California to the Pacific plate. Tectonics 8(1):99–115. https://doi.org/10.1029/TC008i001p00099

Sutherland FH, Kent GM, Harding AJ, Umhoefer PJ, Driscoll NW, Lizarralde D, Fletcher JM, Axen JG, Holbrook WS, González-Fernández A, Lonsdale P (2012) Middle Miocene to early Pliocene oblique extension in the southern Gulf of California. Geosphere 8(4):752–770. https://doi.org/10.1130/GES00770.1

Teske AP, Lizarralde D, Höfig TW, Aiello IW, Ash JL, Bojanova DP, Zhuang G (2020) Expedition 385 preliminary report: Guaymas Basin tectonics and biosphere. IODP Prelim Report. https://doi.org/10.14379/iodp.pr.385.2020

Umhoefer PJ (2011) Why did the Southern Gulf of California rupture so rapidly?—Oblique divergence across hot, weak lithosphere along a tectonically active margin. Geol Soc Am (GSA) Today 21(11):4–10. https://doi.org/10.1130/G133A.1

Umhoefer PJ, Darin MH, Bennett SE, Skinner LA, Dorsey RJ, Oskin ME (2018) Breaching of strike-slip faults and successive flooding of pull-apart basins to form the Gulf of California seaway from ca 8–6 Ma. Geology 46(8):695–698. https://doi.org/10.1130/G40242.1

Umhoefer PJ, Plattner C, Malservisi R (2020) Quantifying rates of "rifting while drifting" in the southern Gulf of California: the role of the southern Baja California microplate and its eastern boundary zone. Lithosphere 12(1):122–132. https://doi.org/10.1130/L1132.1

van Wijk J, Axen G, Abera R (2017) Initiation, evolution and extinction of pull-apart basins: implications for opening of the Gulf of California. Tectonophysics 719:37–50. https://doi.org/10.1016/j.tecto.2017.04.019

Wang Y, Forsyth DW, Savage B (2009) Convective upwelling in the mantle beneath the Gulf of California. Nature 462(7272):499–501. https://doi.org/10.1038/nature08552

Wang Y, Forsyth DW, Rau CJ, Carriero N, Schmandt B, Gaherty JB, Savage B (2013) Fossil slabs attached to unsubducted fragments of the Farallon plate. Proc Natl Acad Sci 110(14):5342–5346. https://doi.org/10.1073/pnas.1214880110

Wernicke B (1981) Low-angle normal faults in the Basin and Range Province: nappe tectonics in an extending orogen. Nature 291(5817):645–648. https://doi.org/10.1038/291645a0

Wernicke B, Axen GJ (1988) On the role of isostasy in the evolution of normal fault systems. Geology 16(9):848–851. https://doi.org/10.1130/0091-7613(1988)016%3C0848:OTROII%3E2.3.CO;2

Wright NM, Seton M, Williams SE, Mueller RD (2016) The Late Cretaceous to recent tectonic history of the Pacific Ocean basin. Earth Sci Rev 154:138–173. https://doi.org/10.1016/j.earscirev.2015.11.015

Wu JE, McClay K, Whitehouse P, Dooley T (2009) 4D analogue modelling of transtensional pull-apart basins. Mar Pet Geol 26(8):1608–1623. https://doi.org/10.1016/j.marpetgeo.2008.06.007

Yilmaz Ö (2001) Seismic data analysis: processing, inversion, and interpretation of seismic data. Soc Explor Geophys. https://doi.org/10.1190/1.9781560801580

Zhao D (2004) Global tomographic images of mantle plumes and subducting slabs: insight into deep Earth dynamics. Phys Earth Planet Inter 146(1–2):3–34. https://doi.org/10.1016/j.pepi.2003.07.032